

A mechanism for the extension and unfolding of parallel telomeric G-quadruplexes by human telomerase at single-molecule resolution

Bishnu P. Paudel^{1,2†}, Aaron Lavel Moye^{3,10†}, Hala Abou Assi⁴, Roberto El-Khoury⁴, Scott B. Cohen³, Monica L. Birrento^{1,2}, Siritron Samosorn⁵, Kamthorn Intharapichai⁶, Christopher G. Tomlinson³, Marie-Paule Teulade-Fichou^{7,8}, Carlos González⁹, Jennifer L. Beck^{1,2}, Masad J. Damha⁴, Antoine M. van Oijen^{1,2*}, and Tracy M. Bryan^{3*}

¹*Molecular Horizons and School of Chemistry and Molecular Bioscience, University of Wollongong, Wollongong, NSW 2522, Australia*

²*Illawara Health and Medical Research Institute, Wollongong, NSW 2522, Australia*

³*Children's Medical Research Institute, University of Sydney, Westmead, New South Wales 2145, Australia*

⁴*Department of Chemistry, McGill University, Montreal, QC H3A 0B8, Canada*

⁵*Department of Chemistry and Center of Excellence for Innovation in Chemistry, Faculty of Science, Srinakharinwirot University, Bangkok 10110, Thailand*

⁶*Department of Biobased Materials Science, Kyoto Institute of Technology, Matsugasaki, Sakyo-ku, Kyoto 606-8585, Japan*

⁷*Institut Curie, PSL Research University, CNRS-UMR 9187, INSERM U1196, F-91405 Orsay, France*

⁸*Université Paris Sud, Université Paris-Saclay, CNRS-UMR 9187, INSERM U1196, F-91405 Orsay, France*

⁹*Instituto de Química Física 'Rocasolano', CSIC, 28006 Madrid, Spain*

¹⁰*Present address: Stem Cell Program and Divisions of Hematology/Oncology and Pulmonary & Respiratory Diseases, Boston Children's Hospital, Harvard Stem Cell Institute, and Department of Genetics, Harvard Medical School, Boston, MA, USA*

[†]*Joint first author*

*Corresponding authors; tbryan@cmri.org.au and vanoijen@uow.edu.au

1 **Abstract**

2 Telomeric G-quadruplexes (G4) were long believed to form a protective structure at telomeres,
3 preventing their extension by the ribonucleoprotein telomerase. Contrary to this belief, we have
4 previously demonstrated that parallel-stranded conformations of telomeric G4 can be extended
5 by human and ciliate telomerase. However, a mechanistic understanding of the interaction of
6 telomerase with structured DNA remained elusive. Here, we use single-molecule fluorescence
7 resonance energy transfer (smFRET) microscopy and bulk-phase enzymology to propose a
8 mechanism for the resolution and extension of parallel G4 by telomerase. Binding is initiated
9 by the RNA template of telomerase interacting with the G-quadruplex; nucleotide addition then
10 proceeds to the end of the RNA template. It is only through the large conformational change
11 of translocation following synthesis that the G-quadruplex structure is completely unfolded to
12 a linear product. Surprisingly, parallel G4 stabilization with either small molecule ligands or
13 by chemical modification does not always inhibit G4 unfolding and extension by telomerase.
14 These data reveal that telomerase is a parallel G-quadruplex resolvase.

1 Human chromosomes contain many guanine (G)-rich elements capable of forming four-
2 stranded G-quadruplex (G4) structures (1-4). A planar G-quartet is formed when four Gs form
3 hydrogen bonds in a cyclical manner via their Hoogsteen faces; such G-quartets stack on top
4 of each other and form G-quadruplexes (5, 6). G-rich sequences are primarily located in
5 promoter regions, intron and exon boundaries, origins of replication and telomeres (1-4).
6 Vertebrate telomeres consist of many tandem repeats of the sequence TTAGGG, comprising a
7 double-stranded region and a 3' G-rich overhang (7). Fluorescence microscopy studies have
8 shown the existence of G4 structures at the telomeric regions of fixed human cells using G4-
9 specific antibodies or stabilizing ligands (8, 9). *In vitro*, telomeric DNA can adopt many
10 different conformations of G4, including inter- or intramolecular forms, arranged in parallel or
11 anti-parallel orientation depending upon the directionality of the DNA backbone (10).
12 Conditions that may mimic those in the nucleus, including high DNA concentration and water
13 depletion, favour parallel conformations of human telomeric G4 (11-13). However, the *in vivo*
14 conformation(s) and biological significance of telomeric G4 in human cells remain elusive and
15 undetermined.

16 Telomere shortening occurs with every cell division in normal human somatic cells, since
17 conventional DNA polymerases cannot completely synthesize the telomeric end (14-16).
18 Telomerase, a telomere-specific ribonucleoprotein enzyme complex, extends telomeric DNA
19 in cancer cells, stem cells and cells of the germline, using a unique mechanism of processive
20 rounds of reverse transcription (17-22). Human telomerase minimally consists of the highly
21 conserved telomerase reverse transcriptase protein (hTERT) and an RNA component
22 containing an 11 nucleotide (nt) template sequence (hTR) (23). Telomerase extends its
23 telomeric substrate by first binding to telomeric DNA, followed by hybridization of the RNA
24 template with the DNA. Second, telomerase extends the substrate DNA by using its RNA as a
25 template for nucleotide addition to the DNA 3' end. Once the template 5' boundary has been

1 reached, telomerase translocates downstream, resulting in re-alignment of the RNA template
2 with the new 3' end of the product DNA (19, 22).

3 One function of telomeric G4 may be to act as a 'cap', protecting the telomere from DNA
4 degradation (24). It has been widely believed that G4 formation within the 3' telomeric
5 overhang blocks telomere extension by telomerase, since early *in vitro* studies had shown that
6 G4 structures inhibit telomerase extension of a telomeric DNA substrate (25, 26). In addition,
7 stabilization of G4 with small-molecule ligands has been shown to more effectively inhibit
8 telomerase activity, suggesting that chemical stabilization of G4 structures may be a viable
9 anti-cancer therapeutic strategy (27-29). However, the above-mentioned studies did not
10 distinguish between G4 conformations, and used oligonucleotides that likely folded into anti-
11 parallel or 'hybrid' G4 forms as a telomerase substrate. A variety of helicases, such as RECQ5,
12 WRN, BLM, FANC-J and RHAU, recognize and resolve G4 in a conformation-specific
13 manner (30-33). Similarly, we have demonstrated that telomerase can bind and extend specific
14 conformations of telomeric G4 - those that are parallel-stranded and intermolecular - and that
15 this property of telomerase is well conserved from ciliates to human (34-36). This suggests that
16 if telomeric G-quadruplexes were to adopt a parallel conformation *in vivo*, they may indeed be
17 extended by telomerase, contrary to what had been previously hypothesized.

18 Telomerase extension reactions in the presence of individual nucleotides demonstrated that the
19 3' end of a G4 substrate aligns correctly with the RNA template of telomerase, suggesting that
20 at least partial resolution of G4 structure is required for telomerase extension (34). However,
21 the evidence for partial disruption of the G4 was indirect, and a mechanistic understanding of
22 telomerase resolution of G4 DNA, in the absence of a known helicase function of hTERT,
23 remained elusive. Furthermore, since all previously-tested substrates were both parallel-
24 stranded and intermolecular, it was unknown which of these properties form the basis of
25 telomerase recognition. To directly study the mechanistic details of parallel G4 unfolding and

1 extension by human telomerase, here we combined ensemble telomerase enzymatic assays and
2 single-molecule FRET (smFRET) measurements *in vitro*, using both intramolecular and
3 intermolecular parallel G4 as FRET sensors. We provide direct evidence that wild-type human
4 telomerase can unfold both intra- and intermolecular parallel G4 completely in the presence of
5 dNTPs, using a 3-step mechanism. First, telomerase binds the G4, partially changing its
6 conformation in a process that involves binding of the hTR template sequence. Second,
7 telomerase adds individual nucleotides to the 3' end of the partially unfolded parallel G4.
8 Lastly, the translocation of telomerase results in complete disruption of the G4 structure.
9 Unexpectedly, stabilization of parallel intermolecular G4 using different G4 ligands did not
10 inhibit telomerase unfolding and extension of this substrate. Overall, we provide a mechanistic
11 explanation of conformation-specific telomerase extension of telomeric G4 at single-molecule
12 resolution and demonstrate that small molecule-mediated inhibition of telomerase extension of
13 telomeric G4 is topology-dependent.

14

15 **Results**

16 **Human telomerase binds, unfolds and extends intramolecular parallel G-quadruplexes**

17 Parallel, intermolecular G4 are substrates for telomerase, whereas intramolecular antiparallel
18 or hybrid conformations are not (25, 26, 34, 35, 37). Determining whether it is the parallel or
19 intermolecular nature of G4 structures that allows their recognition by telomerase has been
20 difficult, since a 4-repeat human telomeric oligonucleotide does not readily fold into stable
21 parallel intramolecular G4 at the concentrations used in *in vitro* assays, and instead exists as a
22 mixture of topologies under most conditions (38-41). For this reason, we made use of the
23 modified nucleotide 2'-fluoro-arabinoguanosine (2'F-araG), which induces parallel propeller-
24 type G4 conformations (42). We have previously demonstrated that substitution of six

1 guanosines in the telomeric sequence AGGG(TTAGGG)₃ with 2'F-araG leads to a 15°C
2 increase in T_m of the resulting intramolecular G4, and a shift from the usual antiparallel or
3 hybrid topology of this sequence (11, 43) to a parallel conformation (Figure 1a) (44). Here, we
4 demonstrate that G4 formed from the unmodified sequence (22G0) in KCl is a poor telomerase
5 substrate, leading to the previously-observed stuttering pattern (26) in a direct telomerase
6 extension assay involving incorporation of radiolabeled $\alpha^{32}\text{P}$ -dGTP (Figure 1b). Substitution
7 with 2'F-araG (22G3; see Supplementary Table 1 for sequence) restored the expected 6-nt
8 repeat pattern of telomerase extension (Figure 1b), despite the increase in thermal stability of
9 this G4. Thus, telomerase is able to extend parallel G4 structures, whether they are inter- or
10 intramolecular.

11 To determine the mechanism of extension of intramolecular G4, we designed a version of 22G3
12 with a FRET donor dye (AlexaFluor 555TM) on one of the propeller loops, and an extended 5'
13 tail; circular dichroism (CD) spectroscopy demonstrated that the G4 formed from this sequence
14 retained a predominantly parallel topology (Supplementary Table 1 and Figure 1c,d;
15 oligonucleotide 22G3+tail). The extended 5' tail enabled hybridization with a second DNA
16 oligonucleotide containing a FRET acceptor dye (AlexaFluor 647TM) and a biotin for surface
17 immobilization in smFRET studies; we refer to the assembled FRET-modified G4 as F-22G3
18 (Figure 1c). F-22G3 also retained a parallel G4 topology, with a slight shoulder at ~290 nm
19 attributable to the duplex portion of the molecule (Figure 1d). Assembled F-22G3 was
20 efficiently extended by telomerase, and was possibly an even better substrate than 22G3, with
21 the expected 6-nt repeat pattern (Figure 1b).

22 We predicted that this structure would yield a high FRET ratio as the donor and acceptor
23 fluorophores would be in close proximity (Figure 1c), but when unfolded the strands would
24 move apart and a low FRET ratio would be expected. We carried out smFRET experiments

1 using the modified F-22G3 construct by tethering it on pegylated coverslips via a biotin-
2 streptavidin-biotin linkage. Surface-immobilized G4s were excited using a 532 nm laser and
3 signals emitted from both the donor and acceptor fluorophores were collected and their
4 intensities measured over time (Figure 1e, top panel); both dyes provided a constant
5 fluorescence signal over several minutes. The apparent FRET values between these two
6 fluorophores were calculated by dividing the acceptor intensity by the sum of the donor and
7 acceptor intensities (Figure 1e, bottom panel). Individual F-22G3 molecules all displayed a
8 constant FRET ratio over time, indicating that they did not undergo any detectable
9 conformational changes in the experimental time window. Using ~100 such smFRET
10 trajectories pooled from multiple independent experiments (sample sizes for each condition
11 indicated in figure panels), a FRET heat map was constructed, showing the distribution of
12 average FRET values (Figure 1f). The heat map showed that the mean FRET value ($0.53 \pm$
13 0.05) remained unchanged over time; an alternative histogram representation of the same data
14 grouped into 15 s bins confirms this conclusion (Supplementary Figure 1a). These data
15 demonstrate that F-22G3 is stable over time.

16 Next, we tested whether telomerase presence affects the F-22G3 structure. To this end, we
17 imaged F-22G3 in the presence of catalytically active telomerase, but in the absence of
18 deoxynucleotide triphosphates (dNTPs). Approximately 65% of F-22G3 molecules showed an
19 abrupt drop in FRET value, from 0.53 ± 0.05 to 0.3 ± 0.1 , during the 160 s after telomerase
20 was injected into the microscopic channel containing immobilized F-22G3 (Figure 1g). The
21 remaining 35% of molecules did not show any change in FRET signal over the observed time;
22 it is possible that the binding reaction had not proceeded to completion within this time period,
23 or that a subpopulation of enzyme or DNA molecules are incompetent for binding. We
24 collected 125 molecules showing a step-wise change in FRET value and plotted the data in a
25 FRET heat map and a histogram plot as a function of time; both plots showed a drop in mean

1 FRET value from ~ 0.53 to ~ 0.3 FRET over this time (Figure 1h and Supplementary Figure
2 1b). We interpret this to represent telomerase binding to F-22G3 and partially opening the
3 structure, which then remained stable in its new conformation.

4 We confirmed this conclusion by quantitatively analyzing the FRET changes during the
5 transitions. For all molecules that showed a change in FRET signal over time, the frequency
6 with which molecules transitioned between states was determined using state finding algorithm
7 vbFRET (<https://sourceforge.net>). Then, the transition frequencies were plotted as a function
8 of initial and final FRET states to obtain transition density plots (TDP) (Figure 1i). In the
9 presence of telomerase, the TDP showed a single cluster of transitions at initial FRET ~ 0.5 and
10 final FRET ~ 0.3 , consistent with the shift in mean FRET in the heat map.

11 To examine changes in F-22G3 structure during its extension by telomerase, we performed
12 smFRET experiments in the presence of both telomerase and dNTPs. Under these conditions,
13 $\sim 65\%$ of molecules showed a two-step drop in FRET values, from 0.53 ± 0.05 to 0.3 ± 0.1 , and
14 then to 0.15 ± 0.05 (Figure 1j-m, and Supplementary Figure 1c, d). The FRET decrease from
15 high to low FRET states in these events was irreversible, supported by the presence of two off-
16 diagonal clusters in the TDP (Figure 1l), suggesting a continuous irreversible unfolding of G4
17 structure. As a control, we performed smFRET experiments in the presence of dNTPs alone
18 and observed no change in FRET signal (Supplementary Figure 1e). These data suggest that
19 telomerase disrupts F-22G3 structure completely in the presence of dNTPs.

20 The rate of F-22G3 unfolding upon telomerase binding in the presence of dNTPs was measured
21 by integrating the dwell time distribution at the 0.3 FRET state ($\tau_{\text{unfolding}}$; Figure 1j) and fitting
22 the distribution to a single-exponential decay (Figure 1n). F-22G3 molecules exhibited
23 telomerase-mediated unfolding with a rate constant of $k_{\text{unfolding}} = 0.050 \pm 0.002 \text{ s}^{-1}$ (mean \pm
24 SEM, $n = 76$ molecules), indicating that there is only one rate-limiting step during the unfolding

1 process. This unfolding rate is comparable with the rate of unfolding of parallel G4 by Pif1
2 helicase (0.11 s^{-1}) (45).

3 **Human telomerase also binds, unfolds and extends intermolecular parallel G-** 4 **quadruplexes**

5 We have previously demonstrated that a tetrameric, parallel G4 (46) formed from four copies
6 of the 7-mer telomeric sequence TTAGGGT in K^+ is highly stable but can be extended by
7 human telomerase (34). This sequence provides the advantage that the conformation of its G4
8 topology is unambiguous; the sequence is too short to form intramolecular G4 structures, and
9 can only exist as a parallel tetramer. To examine whether this tetramer is extended by
10 telomerase using the same mechanism as an intramolecular G4, we prepared a version of this
11 quadruplex labeled with a pair of FRET dyes and a biotin with which to immobilize the DNA.
12 Four different strands, each consisting of the sequence TTAGGGT (here called 7GGT) and a
13 hexa-ethylene glycol spacer, were annealed in an equimolar mixture in KCl solution. Three of
14 these strands were 5' modified with either AlexaFluor 555TM (donor dye), AlexaFluor 647TM
15 (acceptor dye) or biotin, and the remaining strand was unmodified (Figure 2a). We assembled
16 an equimolar mixture of each of these modified oligonucleotides to produce G4s with different
17 combinations of modifications. The resulting mixture of G4s were all parallel-stranded, as
18 confirmed using CD spectroscopy (Supplementary Figure 2a), and had an average melting
19 temperature similar to that of the unmodified G4 ([7GGT]₄; Supplementary Figure 2b). Direct
20 telomerase activity assays demonstrated that human telomerase can extend the FRET-modified
21 G4 construct (which we refer to as F-[7GGT]₄) as efficiently as the unmodified [7GGT]₄
22 (Figure 2b). In single-molecule microscopy analyses, we analyzed only G4 structures
23 containing a single copy of each of the four strands, through selection during post-image
24 processing and data analysis. Note that there are two possible orientations of the positions of
25 the two dyes (on adjacent strands or on diagonally opposite strands, as depicted in Figure 2a),

1 but it is unlikely that the distance between the dyes in these two conformations is sufficiently
2 different to resolve by FRET.

3 smFRET experiments showed that F-[7GGT]₄ exhibits a steady FRET signal at a ratio of ~0.6,
4 and the FRET signal did not change over time (Figure 2c,d, Supplementary Figure 2c),
5 indicating formation of a stable parallel intermolecular G4. Telomerase alone was sufficient
6 for partial unwinding of parallel F-[7GGT]₄, as demonstrated by a drop in FRET state from
7 ~0.6 to ~0.4 with time (Figure 2f-h, Supplementary Figure 2d). About 60% of molecules
8 showed this one-step drop in FRET signal upon injection of telomerase (Figure 2e). Note that
9 the distribution of initial FRET values of those molecules that show a change in FRET value
10 is not as broad as the FRET distribution of the whole population of molecules (compare the
11 spread at 0 time in Figure 2g to that in Figure 2d), supporting the interpretation that those G-
12 quadruplexes that do not bind to telomerase have folded improperly or are folding
13 intermediates, and thus show a high level of dynamic behaviour that is too fast to resolve and
14 results in a broadening of the FRET peak. In the case of the 60% of molecules that do show a
15 drop in FRET signal, we interpret this to demonstrate that telomerase results in a partial
16 separation of the FRET dyes upon binding to one strand of the tetrameric G4.

17 In the presence of telomerase and dNTPs, most F-[7GGT]₄ molecules experienced a two-step
18 drop in FRET, from 0.57 ± 0.05 to 0.36 ± 0.04 , and then to 0.19 ± 0.05 (Figure 2i-k,
19 Supplementary Figure 2e-f); this transition did not occur in the presence of dNTPs alone
20 (Supplementary Figure 2g). The two FRET transition clusters observed by TDP analysis
21 (Figure 2k) suggest that telomerase unfolds parallel intermolecular G4 irreversibly. The rate of
22 unfolding of F-[7GGT]₄ by telomerase in the presence of dNTPs was measured by plotting the
23 dwell times of the intermediate transition states (FRET value of 0.4) and fitting them to a single
24 exponential equation that yielded $k_{\text{unfolding}} = 0.055 \pm 0.003 \text{ s}^{-1}$ (mean \pm SEM, n = 55 molecules;

1 Figure 2l). Thus, the rate of unfolding of [7GGT]₄ by telomerase in the presence of dNTPs is
2 comparable to that of F-22G3.

3 **Complete G-quadruplex unwinding by telomerase requires its catalytic activity**

4 Next, we asked if either of the two step-wise drops in FRET values are dependent upon the
5 nucleotide incorporation activity of telomerase. Synthesis activity requires three conserved
6 aspartate residues in the reverse transcriptase domain of the TERT protein (47-50). Mutation
7 of any one of these aspartates results in loss of telomerase catalytic activity but retention of its
8 ability to bind to a DNA primer (51). We introduced an aspartate-to-alanine mutation at hTERT
9 amino acid 712 and confirmed that this mutant telomerase (D712A) lost all primer extension
10 activity (Supplementary Figure 3a). smFRET experiments with F-[7GGT]₄ demonstrated an
11 initial drop in FRET after addition of D712A telomerase, but no further drop in FRET was
12 observed upon addition of dNTPs (Figure 3a-e). This result suggests that binding of telomerase
13 to F-[7GGT]₄, resulting in partial G4 unwinding, is independent of telomerase catalytic
14 activity, but full unwinding of the G4 requires its extension by telomerase.

15 **The RNA template sequence is involved in partial unfolding of G-quadruplex structure**

16 It is known that the RNA template of telomerase plays an important role in recognizing and
17 binding the telomeric end by canonical base pairing. We have previously demonstrated that
18 [7GGT]₄ is extended by the nucleotides that would be predicted from canonical base-pairing
19 with the RNA template (34). Therefore, we hypothesized that the RNA template binds to the
20 G4, facilitating the opening of the structure. To test this, we performed smFRET experiments
21 in the presence of a 10-nt RNA oligonucleotide mimicking the human telomerase template
22 sequence, RNA.10C (Supplementary Table 1). At a high concentration of RNA.10C (500 μM),
23 a majority of F-[7GGT]₄ molecules executed a single-step drop in FRET from 0.57 to 0.36
24 (Figure 3f, g, j); thus, a short oligonucleotide resembling the telomerase template induces G4

1 unfolding in a similar manner to the whole telomerase enzyme. The fraction of the G4
2 population that showed a drop in FRET signal was dependent on the concentration of RNA.10C
3 (Supplementary Figure 3b, c), providing evidence for direct unwinding of the G4 by the
4 oligonucleotide, rather than passive trapping of a spontaneously unfolded structure.
5 Supporting this conclusion, the effect on G4 structure was very specific to RNA; the presence
6 of 500 μ M of a 10-nt DNA oligonucleotide of identical sequence (DNA.10C) did not stimulate
7 any change in the FRET signal of F-[7GGT]₄ over the same time period (Figure 3h-j). These
8 data suggest that the hTR template is specifically involved in binding to the G4, leading to
9 partial opening of the structure.

10 **Telomerase translocation leads to complete unfolding of G-quadruplex structure**

11 The second step of telomerase-mediated unfolding of G4 DNA requires telomerase catalytic
12 activity (Figure 3c-e). To probe the mechanism for this, we incubated telomerase with F-22G3
13 in the presence of subsets of dNTPs. The first three nucleotides that are incorporated by
14 telomerase at the 3' end of F-22G3 are dTTP, dATP and dGTP, as dictated by the telomerase
15 RNA template sequence (see Figure 4a, e, i). We first carried out extension reactions in the
16 presence of only ddTTP, a chain terminator that inhibits further elongation of the 3' end after
17 its incorporation, and no other nucleotides (Figure 4a). Under these conditions, F-22G3
18 exhibited a FRET drop from \sim 0.5 to \sim 0.3 and remained in the \sim 0.3 FRET state over the
19 remainder of the observation time window (Figure 4b-d and Supplementary Figure 4a). A
20 similar change in FRET from \sim 0.5 to \sim 0.3 was observed when the only nucleotides in the
21 reaction were dTTP and ddATP (Figure 4f-h and Supplementary Figure 4a). However, in the
22 presence of dTTP, dATP and ddGTP, a second step-wise drop in FRET was exhibited by F-
23 22G3, from \sim 0.3 to \sim 0.15 (Figure 4j-l and Supplementary Figure 4a). These data demonstrate
24 that complete G4 unfolding occurs after the addition of three nucleotides complementary to the

1 template; at this point, the template boundary is reached and translocation of the DNA to the 3'
2 region of the template would occur (Figure 4i).

3 **Stable intermolecular, parallel G4 is unfolded and extended by telomerase using a similar** 4 **mechanism**

5 We next asked whether telomerase-mediated unfolding of intermolecular G4 occurs via a
6 similar mechanism to that of intramolecular G4. To address this, we performed smFRET
7 experiments in the presence of subsets of dNTPs and observed the change in FRET signal
8 displayed by F-[7GGT]₄ over time (Supplementary Figure 4b-k). The FRET signal dropped in
9 a single step, from ~0.6 to ~0.4, in the presence of telomerase and either ddTTP alone
10 (Supplementary Figure 4c-e) or dTTP and ddATP (Supplementary Figure 4f-h). However, in
11 the presence of telomerase and dTTP, dATP and ddGTP, a two-step decrease was observed,
12 from a high FRET state (~0.6) to ~0.4 and then to the lowest FRET state (~0.2) (Supplementary
13 Figure 4b, i-k). Overall, these data demonstrate that telomerase binds and unfolds parallel G4
14 using a similar mechanism, whether the strand topology is intramolecular or intermolecular.

15 **Ligand stabilization of intramolecular parallel G4 partially inhibits but does not prevent** 16 **G4 unwinding by telomerase**

17 Antiparallel or hybrid telomeric G4 are not efficiently used as substrates by telomerase, and
18 their stabilization with small molecule G4-binding ligands can further decrease the ability of
19 telomerase to extend them (28, 29). We therefore sought to determine whether a ligand-
20 mediated increase in stability of parallel G4 affects their extension by telomerase. To this end,
21 we used three different G4-stabilizing compounds: the porphyrin N-methyl mesoporphyrin IX
22 (NMM) (52, 53), the berberine derivative SST16 (54, 55) and the bisquinolinium compound
23 PhenDC3 (56, 57) (Supplementary Figure 5a-c). CD spectroscopy confirmed that none of the
24 ligands substantially changed the overall parallel G4 conformation of F-22G3 (Supplementary

1 Figure 5d-f), and melting assays showed dramatic thermal stabilization of this G4 upon binding
2 by all three ligands (ΔT_m of $>25^\circ\text{C}$ (NMM), $+11^\circ\text{C}$ (SST16) and $>25^\circ\text{C}$ (PhenDC3), under the
3 conditions detailed in Supplementary Figure 5d-i). SST16 caused a decrease in signal of the
4 peak at 260 nm that may be attributable to the association between the ligand and the G-
5 quartets, resulting in slight changes in stacking interactions without a change in overall
6 topology (58, 59). The ligands did not change the steady smFRET signal of F-22G3 in the
7 absence of telomerase (Supplementary Figure 5j-o). In the presence of telomerase and dNTPs,
8 the number of molecules experiencing a two-step FRET decrease was reduced by about 2-fold;
9 nevertheless, 25 – 30% of molecules showed the same FRET decrease from ~ 0.5 to ~ 0.3 and
10 then to ~ 0.15 as in the absence of ligands (Figure 5a-j). The rates of telomerase-mediated
11 unfolding of NMM-, SST16- and PhenDC3-stabilized F-22G3 were $0.018 \pm 0.005 \text{ s}^{-1}$, $0.032 \pm$
12 0.005 s^{-1} , and $0.034 \pm 0.004 \text{ s}^{-1}$, respectively (mean \pm SEM; Figure 5k), which were all
13 significantly slower ($p < 0.0001$, $p = 0.0002$ and $p = 0.0002$, respectively; Student's t-test) than
14 in the absence of ligands ($0.050 \pm 0.002 \text{ s}^{-1}$). The reduced rate of G4 unfolding provides
15 evidence that most or all of these molecules were bound by ligands, but that ligand presence
16 slowed the rate of their unfolding by telomerase. Consistent with these data, all three ligands
17 partially inhibited telomerase extension of F-22G3 when incubated at the same concentrations
18 in ensemble telomerase activity assays (Figure 5l). We therefore conclude that telomerase
19 unfolding and extension of an intramolecular parallel G4 are partially inhibited by ligand
20 stabilization; nevertheless, telomerase is able to overcome this stabilization and unwind a
21 substantial proportion (25 – 30%) of molecules (Figure 5j).

22 **Ligand stabilization of intermolecular parallel G4 does not inhibit telomerase activity or** 23 **telomerase-mediated G4 unfolding**

24 To determine the generality of the ability of telomerase to extend G4 in the presence of
25 stabilizing ligands, we also incubated $[\text{7GGT}]_4$ with the same three G4 ligands. CD

1 spectroscopy confirmed that none of the ligands substantially changed the parallel G4
2 conformation of [7GGT]₄ (Supplementary Figure 6a, c, e). Melting assays showed dramatic
3 thermal stabilization of [7GGT]₄ upon binding by all three ligands (ΔT_m of +13°C (NMM),
4 +21°C (SST16) and +26°C (PhenDC3), under the conditions detailed in Supplementary Figure
5 6a-f). Telomerase activity assays were carried out at the same concentrations of [7GGT]₄ and
6 each ligand as used in CD analyses; surprisingly, stabilization of the G-quadruplex did not
7 inhibit its extension by telomerase, and activity was even slightly increased when [7GGT]₄ was
8 stabilized by NMM (Figure 6a–c). As previously described (29), PhenDC3 caused a decrease
9 in enzyme processivity after the addition of 4 telomeric repeats to either a linear or a G4
10 substrate, most likely resulting from G-quadruplex stabilization within the product DNA
11 (Figure 6c). Concentrations of PhenDC3 higher than 1 μ M caused dramatic inhibition of
12 activity (Supplementary Fig. 6i), but again this effect was observed with both linear and G4
13 substrates, indicating G4-independent direct inhibition of telomerase by PhenDC3, as
14 previously described (29). Neither NMM nor SST16 inhibited extension of linear or G4
15 substrates at any concentration used (Supplementary Figures 6g,h). Thus, substantial
16 stabilization of a parallel intermolecular G4 by three different ligands did not inhibit the ability
17 of telomerase to use the G4 as a substrate.

18 To further understand this effect at the molecular level we performed smFRET experiments to
19 visualize F-[7GGT]₄ stabilized by NMM, SST16 or PhenDC3 in the presence of telomerase,
20 with or without dNTPs. Ligand-stabilized F-[7GGT]₄ exhibited a constant FRET signal at 0.57
21 (Supplementary Figure 6j-o), but in the presence of telomerase, a single-step FRET decrease
22 from 0.57 to 0.36 was observed in a majority of single-molecule traces (Figure 6d,
23 Supplementary Figures 6p-u). These data suggest that ligand binding to F-[7GGT]₄ did not
24 prevent telomerase from inducing a conformational change in the G4, as occurs in the absence
25 of ligand. When F-[7GGT]₄ was incubated with both telomerase and dNTPs in the presence of

1 each ligand, most molecules showed a unidirectional two-step decrease in FRET value, from
2 0.57 to 0.36, and then to 0.19 (Figure 6d-m). We assessed the F-[7GGT]₄ unfolding rate in the
3 presence of the ligands by measuring the dwell time of each molecule in the transient
4 intermediate state (0.36 FRET) and fitting time distributions with a single exponential equation.
5 The rates of telomerase-mediated unfolding of NMM-, SST16- and PhenDC3-stabilized G4
6 were $0.085 \pm 0.004 \text{ s}^{-1}$, $0.088 \pm 0.004 \text{ s}^{-1}$, and $0.032 \pm 0.001 \text{ s}^{-1}$, respectively (mean \pm SEM;
7 Supplementary Figure 6v). Thus, while PhenDC3 resulted in a decrease in the unfolding rate
8 of this G-quadruplex, in the presence of NMM and SST16 unfolding occurred significantly
9 faster ($p < 0.0001$; Student's t-test) than in the absence of ligands ($0.055 \pm 0.002 \text{ s}^{-1}$). Together,
10 these data demonstrate that neither unwinding nor extension of parallel intermolecular G4 by
11 telomerase were inhibited by ligand-mediated stabilization of the G4.

12

13 **Discussion**

14 Previously, we have shown that highly purified human telomerase can disrupt parallel
15 intermolecular G4 structures and then extend them in a processive manner (34). Here, we
16 provide the first mechanistic details of telomerase resolution of parallel G4 structures. Our data
17 demonstrate that G4 unfolding occurs in three major steps: i) the telomerase template RNA
18 actively invades the G-quartets in order to hybridize with the G-rich DNA, causing partial
19 opening of the G4 structure; ii) telomerase extends the 3' end of this partially unwound
20 structure, adding single nucleotides according to the RNA template, and iii) translocation of
21 telomerase once nucleotide addition has reached the template boundary triggers complete
22 unfolding of the G4 structure (Figure 7). It has previously been difficult to distinguish whether
23 it is the parallel or intermolecular nature of G4 structures that allows their recognition by
24 telomerase. Here, we overcome this difficulty by exploiting the stabilization of intramolecular

1 parallel G4 conferred by the modified nucleotide 2'F-araG (44), enabling the demonstration
2 that inter- and intramolecular parallel G4 are extended by telomerase using the same 3-step
3 mechanism. These data reveal human telomerase to be a parallel G4 resolvase.

4 Several other proteins have been shown to assist telomerase extension of telomeric DNA by
5 resolving antiparallel G4 in the substrate, including telomeric protein POT1 (26, 60), a splice
6 variant of hnRNP A2 (61), and the ciliate protein StyRecQL (62, 63). In contrast, we have
7 verified that highly purified telomerase, free of contaminating helicases or other proteins, is
8 able to extend [7GGT]₄ (34). Therefore, we conclude that telomerase itself has the ability to
9 unwind parallel G4, without the assistance of interacting helicases.

10 Telomerase partially unfolds parallel G4, independently of telomerase catalytic activity, as
11 indicated by the drop in FRET signal upon telomerase association with G4 (Figure 3a-e). The
12 resulting stable intermediate FRET value is consistent with a partial separation of the FRET
13 dyes in the absence of complete strand dissociation; we interpret these data to indicate that
14 binding of telomerase RNA to the nucleotides at the 3' end of one DNA strand allows RNA-
15 DNA hybridization to occur, but the dyes are still sufficiently close together to give a non-zero
16 FRET signal (Figure 7). To investigate whether the template RNA of telomerase plays a critical
17 role in this initial G4 unfolding, we carried out experiments in the presence of a short RNA
18 oligonucleotide with a sequence complementary to the telomere repeat, mimicking the template
19 region of hTR. This RNA molecule was able to partially unfold the structure in a similar
20 manner to the whole enzyme. This observation suggests that it is the RNA component of
21 telomerase, rather than the hTERT protein, that promotes the initial unwinding of parallel G4,
22 followed by hybridization to the 3' end. A DNA oligonucleotide of identical sequence did not
23 promote any G4 unwinding (Figure 3h-j); if oligonucleotide binding was due to passive
24 trapping of a spontaneously-unfolding G4, this would also have been observed in the presence
25 of a DNA C-strand. There are two lines of evidence to suggest that the difference in behaviour

1 of the DNA and RNA oligonucleotides cannot simply be explained by the potentially higher
2 stability of a DNA-RNA hybrid. Firstly, for this to be the case, there would need to be initial
3 binding of either the DNA or the RNA oligonucleotide to the G4 DNA in order to form a
4 hybrid. However, the tetrameric parallel G4s used in these experiments is highly stable; it did
5 not demonstrate any spontaneous unwinding during the observation time of the smFRET
6 experiments, and in our previous work we have shown that the parallel tetrameric G4 did not
7 show any unwinding over the time scale of hours (34). Secondly, the concentration-dependent
8 unfolding by the RNA oligonucleotide (Supplementary Figure 3b, c) also supports an active
9 invasion mechanism. A similar template-mimicking RNA was unable to form a DNA-RNA
10 hybrid with an antiparallel G4 of similar stability to the parallel G4 used in the present study
11 (64), demonstrating that this is a specific interaction between this RNA and parallel G4
12 structures. Single-molecule FRET studies have illuminated the mechanisms used by other G4-
13 unwinding proteins; for example, the helicase RHAU/DHX36 was shown to stack on the top
14 of the G4 plane and bind to the exposed 3' single stranded DNA tail (65), whereas the
15 replication protein RPA has been proposed to bind to G4 structures via their exposed loops
16 (66). Our data demonstrate that telomerase possesses a unique mechanism of G4 resolution,
17 mediated by its integral RNA subunit.

18 Telomerase extends the 3' end of parallel G4 while the G4 remains partially structured, as
19 demonstrated by the intermediate FRET state remaining unchanged until the hTR template
20 boundary was reached. Upon translocation, complete G4 unfolding occurs, represented by a
21 second step-wise drop in FRET signal. One possible explanation for this observation is that the
22 G4 structure needs to pass through the telomerase DNA-binding cleft during the conformation
23 changes required for telomerase translocation, and the resulting steric hindrance results in
24 complete dissociation of the parallel telomeric G4 (Figure 7). It has also been proposed that
25 dissociation of the RNA-DNA hybrid occurs outside the active site, and the realigned hybrid

1 is then re-captured into the active site (67); it is plausible that this recapturing leads to G4
2 dissociation. Our smFRET experiments do not address where RNA/DNA association and
3 dissociation occur, but we hypothesize that steric hindrance encountered by the G4 structure
4 may play a major role in the complete unfolding of the G4, whether this occurs within the
5 catalytic active site or upon re-entry.

6 We used the G4-stabilizing ligands NMM, SST16 and PhenDC3, all of which bind to parallel
7 G4 (53, 54, 68), to understand whether telomerase extension of these structures can be
8 modulated. Despite substantial thermal stabilization of the G4, these ligands did not inhibit
9 telomerase extension of intermolecular parallel telomeric G4, with two of them instead slightly
10 accelerating G4 unfolding. The ligands did reduce the number of intramolecular parallel G4
11 molecules unwound by telomerase; nevertheless, some molecules were unwound by
12 telomerase despite ligand binding, using the same two-step mechanism as in the absence of
13 ligands. The fact that telomerase was able to extend parallel G4 even after substantial thermal
14 stabilization of the structure using either small molecule ligands (Figures 5, 6) or chemical
15 modification (Figure 1) provides further evidence that telomerase is not simply exploiting
16 inherent instability in the G4 structure to passively extend spontaneously unwound DNA, but
17 is instead actively involved in G4 unwinding.

18 NMM has been demonstrated to bind to parallel telomeric G4 by stacking on the outermost G-
19 quartets (69), which would be predicted to interfere with telomerase extension. This
20 observation suggests that, like other proteins such as RHAU helicase (30, 70), telomerase is
21 able to dislodge ligands from the tetramolecular G4 structure while unfolding it. This
22 displacement activity is structure dependent, since telomerase is less able to dislodge ligands
23 from a parallel intramolecular G4, possibly due to the presence of DNA loops. Such a
24 displacement mechanism would have implications for interpreting the biological effects of G4-

1 stabilizing ligands in cell-based studies, since any effects on telomerase action and telomere
2 length will depend on the conformational specificity of the ligand.

3 There is growing evidence for G4 formation at telomeres (8, 34, 71-74). In human cells, it is
4 not known if they form at the 3' end of the telomeric overhang, internally, or a combination of
5 both, or which conformation of G4 occurs at these locations *in vivo*. While in-cell NMR studies
6 of transfected telomeric oligonucleotides detected hybrid and antiparallel structures (75), a
7 study using parallel-specific antibodies reported detection of parallel telomeric G-quadruplexes
8 in human cells (76) and a parallel-specific ligand induces G4 formation at human telomeres
9 (34). It is also possible that different conformations exist at different telomeric overhangs
10 within the same cell. Intermolecular parallel G4 may also form between telomeric overhangs;
11 it has been suggested that tetrameric parallel G-quadruplexes could be responsible for the
12 correct alignment of four chromatids during meiosis (77). Regardless of this uncertainty, our
13 data unequivocally demonstrate that human telomerase interacts directly with parallel G4
14 structures and resolves them. The conserved ability of human and ciliate telomerase enzymes
15 to unwind these structures suggests that parallel G-quadruplexes form at telomeric overhangs
16 *in vivo*, and do not form a barrier to telomerase extension.

17

18 **Methods**

19 **Oligonucleotides and G-quadruplex preparation**

20 Most DNA oligonucleotides (Supplementary Table 1) were purchased from Integrated DNA
21 Technologies and RNA oligonucleotides from Dharmacon, with purification by high
22 performance liquid chromatography (HPLC). Oligonucleotides 22G0, 22G3, and 22G0+tail
23 were synthesized as previously described (44). Synthesis of (C5-alkylamino)-dT-41G3 (the

1 equivalent of 22G3+tail prior to AlexaFluor 555TM conjugation) was performed on an ABI
2 3400 DNA synthesizer (Applied Biosystems) at 1 μ mol scale on Unylinker CPG solid support
3 (Chemgenes). Conjugation of (C5-alkylamino)-dT-41G3 to AlexaFluor 555TM NHS Ester to
4 produce the desired 22G3+tail oligonucleotide was achieved following the standard protocol
5 by Sigma-Aldrich (Protocol for Conjugating NHS-Ester Modifications to Amino-Labeled
6 Oligonucleotides). Briefly, a solution of (C5-alkylamino)-dT-41G3 (200 μ L, 0.3 mM) in
7 sodium tetraborate decahydrate buffer (0.091 M, pH 8.5) was combined with a solution of
8 AlexaFluor 555 in anhydrous DMSO (50 μ L, 8 mM) and the reaction mixture was left shaking
9 at room temperature for 2.5 hours. Samples were evaporated to dryness and the 22G3+tail
10 product was purified by anion exchange HPLC as described (44). The peak of (C5-
11 alkylamino)-dT-41G3 eluted between 24 and 26 min, while the desired product peak of
12 22G3+tail eluted between 27 and 28.5 min. Based on the area of the two peaks, the yield of the
13 conjugation reaction is approximately 25%. The collected sample of 22G3+tail was desalted
14 on NAP-25 desalting columns according to the manufacturer's protocol. The maximum
15 absorbance of AlexaFluor 555 (555 nm) in the purified 22G3+tail was verified with UV-Vis
16 spectroscopy. The mass of 22G3+tail was verified by high resolution liquid chromatography–
17 mass spectrometry (LC–MS; 14,000.23 m/z).

18 Intramolecular G4 formation using 22G0 and derivatives (Supplementary Table 1) was
19 performed at a DNA concentration of 10 μ M in 20 mM potassium phosphate, 70 mM potassium
20 chloride pH 7, 1 mM MgCl₂, by heat denaturing for 10 min at 90 °C, allowing the DNA to cool
21 slowly (~1 h) to 25 °C and equilibration at this temperature for 12-16 h. Formation of
22 fluorescently-labeled F-22G3 with a duplex tail (Figure 1c) involved incubation of 10 μ M each
23 of oligonucleotides 22G3+tail and 647-Strand2 (Supplementary Table 1) under the same
24 folding conditions as given for 22G0.

1 7GGT and its labeled derivates were combined at a final concentration of 1 mM in K⁺ hTel
2 buffer (50 mM Tris-HCl, pH 8, 1 mM MgCl₂, 150 mM KCl) and heat denatured for 5 min at
3 95 °C. They were allowed to cool slowly (~1 h) to 25 °C and left to equilibrate at this
4 temperature for 72 h. Intermolecular G4 formation was confirmed by native gel electrophoresis
5 followed by staining with SYBR® Gold (Life Technologies), as described (34). DNA
6 concentrations were determined by UV absorbance at 260 nm (extinction coefficients in
7 Supplementary Table 1). Concentrations of G-quadruplexes are given as the concentration of
8 assembled complexes (i.e. taking strand stoichiometry into account). Folded G-quadruplexes
9 were stored at 4 °C until use.

10 **Circular dichroism**

11 Circular dichroism (CD) spectra were recorded at 25 °C on either an Aviv 215S or a JASCO
12 J-810 CD spectrometer equipped with Peltier temperature controllers. G-quadruplex samples
13 of the desired conformation were prepared at 250 nM - 20 μM in their folding buffers. Three
14 to four scans were accumulated over the indicated wavelength ranges in a 0.1 cm or 1 cm path
15 length cell. Parameters used with the Aviv CD spectrometer included a time constant of 100
16 ms, averaging time 1 s, sampling every 1 nm, and bandwidth 1 nm, while the JASCO CD
17 spectrometer was used with a scan rate of 100 nm/min and a response time of 2.0 s. Buffers
18 alone were also scanned and these spectra subtracted from the average scans for each sample.
19 CD spectra were collected in units of millidegrees, normalized to the total species
20 concentrations and expressed as molar ellipticity units (deg × cm² dmol⁻¹). Data were smoothed
21 using the Savitzky-Golay function within the JASCO graphing software, or the smoothing
22 function within GraphPad Prism. For thermal stability analysis, the samples were scanned
23 using the above parameters, but with a fixed wavelength (260 nm) over increasing temperature
24 (25 °C to 100 °C), at a rate of ~1 °C/min. For reactions including SST16 or PhenDC3 (prepared
25 as described (54, 56)), the ligand was incubated with the folded DNA substrate at 25 °C for 30

1 min prior to CD spectroscopy. For reactions including NMM (Frontier Scientific, USA), the
2 ligand was incubated with the DNA prior to G-quadruplex folding and the G4-ligand complex
3 diluted prior to CD spectroscopy. Concentrations of ligands and G4 DNA used for each
4 experiment are given in the figure legends.

5 **Preparation of telomerase**

6 Human telomerase was overexpressed in HEK293T cells and purified as described (34, 78).
7 Briefly, plasmids encoding hTERT, hTR and dyskerin (available from the authors with an
8 accompanying Materials Transfer Agreement) were transiently transfected into HEK293T cells
9 growing in 20 L bioreactors using polyethylenimine and cells harvested 4 days later. Cell
10 lysates were clarified, ribonucleoprotein complexes enriched with MgCl₂, and telomerase
11 immunoprecipitated with a sheep polyclonal hTERT antibody, raised against hTERT amino
12 acids 276-294 (ARPAEEATSLEGALSGTRH) (79); available from Abxexa Ltd., Cambridge,
13 UK (catalogue number abx120550). Telomerase was eluted by competitive elution with the
14 same peptide in 20 mM HEPES-KOH (pH 8), 300 mM KCl, 2 mM MgCl₂, 0.1% v/v Triton X-
15 100 and 10% v/v glycerol. Fractions were assayed for telomerase concentration by dot-blot
16 northern against hTR (78), and equal amounts of enzyme (~1.5 nM) used in each activity assay.

17 **Telomerase activity assays**

18 The following reaction was prepared to give 20 µL per sample: 250 nM - 2 µM of the specified
19 oligonucleotide (concentrations given in figure legends), 20 mM HEPES-KOH (pH 8), 2 mM
20 MgCl₂, 150 mM KCl, 5 mM dithiothreitol, 1 mM spermidine-HCl, 0.1% v/v Triton X-100, 0.5
21 mM dTTP, 0.5 mM dATP, 4.6 µM nonradioactive dGTP and 0.33 µM [α -³²P]dGTP at 20 mCi
22 mL⁻¹, 6000 Ci mmol⁻¹ (PerkinElmer Life Sciences). For reactions including SST16 or
23 PhenDC3, the ligand was incubated with the folded DNA substrate at 25 °C for 30 min prior
24 to adding other components. For reactions including NMM, the ligand was incubated with the
25 DNA prior to G-quadruplex folding; concentrations are given in figure legends. Telomerase

1 activity assays were initiated by adding purified human telomerase to ~1.5 nM, and incubating
2 at 37 °C for 1 h. The reaction was quenched by the addition of 20 mM EDTA and $1-2 \times 10^3$
3 cpm of a 5'-³²P-labeled synthetic 100-mer, 30-mer or 12-mer DNA (as indicated in figure
4 legends) as an internal recovery standard. Products of telomerase extension were recovered as
5 described, either with phenol/chloroform extraction followed by ethanol precipitation (34), or,
6 for biotinylated substrates, by recovery with magnetic streptavidin beads (78). The solution
7 was heated at 90 °C for 5 min, and 3 µL was electrophoresed over a 10% polyacrylamide
8 sequencing gel (0.2 mm thick x 40 cm length x 35 cm width, 32-well comb) run in 1 × TBE/8
9 M urea at 85 W. The gel was transferred to filter paper, dried for 30 min at 80 °C, exposed to
10 a PhosphorImager screen, visualized on a Typhoon FLA9500 scanner (GE Healthcare
11 Lifesciences) and analyzed using ImageQuant™ software.

12 **Single-molecule Fluorescence imaging and data analysis**

13 *Microscope setup for FRET imaging*

14 A home-built objective-type total internal reflection fluorescence (TIRF) microscope based on
15 an Olympus IX-71 model was used to record single-molecule movies. A Coherent Sapphire
16 green (532 nm) laser was used to excite donor molecules at an angle of TIRF by focusing on a
17 100X oil immersed objective. FRET was measured by excitation with a 532 nm laser and the
18 emissions at 565 and 665 nm were collected using a band pass filter at 560-600 nm and a long
19 pass filter at 650 nm. Scattered light was removed by using a 560 nm long pass filter.
20 AlexaFluor 555 and AlexaFluor 647 signals were separated by 638 nm dichroic using
21 photometrics dual view (DV-2) and both signals were focused onto a charge-coupled device
22 (CCD) camera (Hamamatsu C9 100-13), simultaneously. Data were collected at 5 frames per
23 second.

1 *Sample preparation for FRET experiments*

2 Quartz coverslips were treated with 100% ethanol and 1 mM KOH. Then, aminosilanization
3 of coverslips was carried out in a 1% v/v (3-Aminopropyl)triethoxy silane (Alfa Aesar,
4 A10668, UK) solution in acetone. PEGylation was carried out by incubating a mixture of
5 biotinPEG-SVA and mPEG-SVA (Laysan Bio, AL, USA) at a ratio of 1:20 prepared in 0.1 M
6 NaHCO₃ solution on the top of a silanized coverslip for at least 3-4 h. Finally, PEGylated
7 coverslips were stored under dry nitrogen gas at -20 °C.

8 *Single-molecule experiments*

9 Immuno-pure Neutravidin solution was prepared in K⁺ buffer (10 mM Tris-HCl (pH 8), 1 mM
10 MgCl₂ and 150 mM KCl) and spread on the top of a dry PEGylated coverslip followed by a 10
11 min incubation. Sample flow chambers were created by sandwiching polydimethylsiloxane
12 (PDMS) on top of the neutravidin coated coverslip. Then, blocking buffer (K⁺ buffer with 1%
13 Tween-20) was injected into the channel in order to reduce non-specific binding of proteins on
14 the surface, followed by 10-15 min incubation. A 50 pM solution of biotinylated FRET G-
15 quadruplex substrate was prepared in K⁺ buffer and 200 μL injected into the flow chamber
16 using a syringe pump (ProSense B.V.) followed by incubation for 10 min. Unbound sample
17 was washed off in K⁺ buffer. Movies were recorded at room temperature (20 ± 1°C) for 3-5
18 minutes in oxygen-scavenging system (OSS) consisting of protocatechuic acid (PCA, 2.5 mM)
19 and protocatechuate-3,4-dioxygenase (PCD, 50 nM) to reduce photo-bleaching of the
20 fluorophores, and 2 mM Trolox to reduce photo-blinking of dyes. For experiments in the
21 presence of enzyme, 200 μL of telomerase (0.5 nM; expressed and purified as described above)
22 and/or dNTPs or ddNTPs (0.5 mM) were injected into the microscopic channel containing
23 immobilized G4 DNA while the movie was recorded continuously. The buffer reached the
24 microscopic channel at ~10 s and the movie was collected until all acceptor molecules
25 photobleached. For reactions including SST16 or PhenDC3, the ligands were incubated with

1 the folded DNA substrate at 25 °C for 30 min prior to dilution for sample injection. For
2 reactions including NMM, the ligand was incubated with the DNA prior to G-quadruplex
3 folding, and the G4-ligand complex diluted to 50 pM G4 prior to injection. Concentrations of
4 DNA and ligands combined for each experiment are given in the figure legends.

5 *Data analysis*

6 Single-molecule intensity time trajectories were generated in IDL (software available at
7 <https://cplc.illinois.edu/software/>) and these trajectories were analyzed in MATLAB using
8 home-written scripts (available from the authors upon request). Approximate FRET value is
9 measured as the ratio of acceptor intensity to the sum of the donor and acceptor intensities after
10 correcting cross talk between donor and acceptor channels. The collected FRET traces were
11 further analyzed using the vbFRET algorithm (<https://sourceforge.net>) to find possible FRET
12 states and transition frequency among these FRET states with a Hidden Markov Model
13 (HMM).

14

15 To measure rate constants for G4 unfolding, integrated dwell time histograms were constructed
16 and fitted to a single exponential decay function of the form:

$$17 \quad y(t) = y_0 + A_1(1 - e^{-k_{obs1} * t})$$

18 where A_1 is the fraction of decay population and k_{obs1} is the apparent observed rate constant.

19 *Gaussian fitting of the cumulative FRET histograms*

20 Multiple-Gaussian fit model was applied to FRET histograms generated by binning many
21 FRET trajectories to obtain mean FRET values.

1 **Acknowledgements**

2 We thank Omesha Perera for plasmid construction, George Lovrecz and Tram Phan for
3 production of telomerase-expressing cells, Timothy Adams for providing pAPEX vectors and
4 for consultation on overexpression of telomerase, and Corinne Getta for preparation of
5 PhenDC3. The work in the Bryan laboratory was supported by Cancer Council NSW project
6 grants RG 11-07 and RG 16-10, a Denise Higgins PhD Scholarship and a Kids Cancer Alliance
7 PhD Top Up Scholarship from Cancer Institute NSW (to A.L.M.). The work in the van Oijen
8 laboratory was supported by an Australian Laureate Fellowship to A.M.v.O. (FL140100027).
9 S.B.C. was supported by the Ernest and Piroška Major Foundation. M.L.B. was supported by
10 an Australian Postgraduate Award. Funding in the Damha laboratory was provided by the
11 National Science and Engineering Council of Canada (Discovery NSERC grant). S.S. was
12 supported by Center of Excellence for Innovation in Chemistry (PERCH-CIC) and Research
13 Unit of Natural Products and Organic Synthesis for Drug Discovery (NPOS 405/2560).

14

15 **Author contributions**

16 The smFRET assay was designed and the study conceived by B.P., A.L.M., A.M.v.O. and
17 T.M.B.; smFRET experiments were performed and analyzed by B.P. and A.M.v.O.; telomerase
18 was purified and ensemble telomerase assays were performed and analyzed by A.L.M., C.G.T.,
19 T.M.B. and S.B.C.; modified oligonucleotide synthesis and characterization were performed
20 by H.A.A., R.E.K., C.G. and M.J.D.; synthesis and characterization of G4 ligands was
21 performed by S.S., K.I., M.L.B., J.L.B. and M.-P. T.-F.; the manuscript was written by B.P.
22 and T.M.B.; and all authors edited the manuscript.

1 **Competing interests**

2 The authors declare no competing interests.

3 **Code availability**

4 The software used for data analysis is freely available at <https://cplc.illinois.edu/software/>

5 (IDL) and <https://sourceforge.net> (vbFRET). The custom MATLAB script used for trajectory

6 analysis is available from the authors upon request.

References

1. Rhodes D, Lipps HJ. G-quadruplexes and their regulatory roles in biology. *Nucleic Acids Res.* 2015;43(18):8627-37.
2. Maizels N, Gray LT. The G4 genome. *PLoS Genet.* 2013;9(4):e1003468.
3. Bochman ML, Paeschke K, Zakian VA. DNA secondary structures: stability and function of G-quadruplex structures. *Nat Rev Genet.* 2012;13(11):770-80.
4. Huppert JL, Balasubramanian S. Prevalence of quadruplexes in the human genome. *Nucleic Acids Res.* 2005;33(9):2908-16.
5. S. Neidle SB. *Quadruplex Nucleic Acids*: Royal Society of Chemistry; 2006.
6. Williamson JR, Raghuraman MK, Cech TR. Monovalent cation-induced structure of telomeric DNA: the G-quartet model. *Cell.* 1989;59(5):871-80.
7. Blackburn EH. Structure and function of telomeres. *Nature.* 1991;350:569.
8. Biffi G, Tannahill D, McCafferty J, Balasubramanian S. Quantitative visualization of DNA G-quadruplex structures in human cells. *Nat Chem.* 2013;5(3):182-6.
9. Gomez D, Wenner T, Brassart B, Douarre C, O'Donohue MF, El Khoury V, . . . Riou JF. Telomestatin-induced telomere uncapping is modulated by POT1 through G-overhang extension in HT1080 human tumor cells. *J Biol Chem.* 2006;281(50):38721-9.
10. Burge S, Parkinson GN, Hazel P, Todd AK, Neidle S. Quadruplex DNA: sequence, topology and structure. *Nucleic Acids Res.* 2006;34(19):5402-15.
11. Renciuik D, Kejnovska I, Skolakova P, Bednarova K, Motlova J, Vorlickova M. Arrangements of human telomere DNA quadruplex in physiologically relevant K⁺ solutions. *Nucleic Acids Res.* 2009;37(19):6625-34.
12. Miller MC, Buscaglia R, Chaires JB, Lane AN, Trent JO. Hydration is a major determinant of the G-quadruplex stability and conformation of the human telomere 3' sequence of d(AG3(TTAG3)3). *Journal of the American Chemical Society.* 2010;132(48):17105-7.
13. Heddi B, Phan AT. Structure of human telomeric DNA in crowded solution. *Journal of the American Chemical Society.* 2011;133(25):9824-33.
14. Olovnikov AM. [Principle of marginotomy in template synthesis of polynucleotides]. *Dokl Akad Nauk SSSR.* 1971;201(6):1496-9.
15. Watson JD. Origin of concatemeric T7 DNA. *Nat New Biol.* 1972;239(94):197-201.
16. Harley CB, Futcher AB, Greider CW. Telomeres shorten during ageing of human fibroblasts. *Nature.* 1990;345(6274):458-60.
17. Greider CW, Blackburn EH. The telomere terminal transferase of *Tetrahymena* is a ribonucleoprotein enzyme with two kinds of primer specificity. *Cell.* 1987;51(6):887-98.
18. Greider CW, Blackburn EH. Identification of a specific telomere terminal transferase activity in *Tetrahymena* extracts. *Cell.* 1985;43(2 Pt 1):405-13.
19. Greider CW, Blackburn EH. A telomeric sequence in the RNA of *Tetrahymena* telomerase required for telomere repeat synthesis. *Nature.* 1989;337(6205):331-7.
20. Greider CW. Telomerase is processive. *Mol Cell Biol.* 1991;11(9):4572-80.

21. Hiyama E, Hiyama K. Telomere and telomerase in stem cells. *Br J Cancer*. 2007;96(7):1020-4.
22. Podlevsky JD, Chen JJ. It all comes together at the ends: telomerase structure, function, and biogenesis. *Mutat Res*. 2012;730(1-2):3-11.
23. Wyatt HD, West SC, Beattie TL. InTERTpreting telomerase structure and function. *Nucleic Acids Res*. 2010;38(17):5609-22.
24. Smith JS, Chen Q, Yatsunyk LA, Nicoludis JM, Garcia MS, Kranaster R, . . . Johnson FB. Rudimentary G-quadruplex-based telomere capping in *Saccharomyces cerevisiae*. *Nat Struct Mol Biol*. 2011;18(4):478-85.
25. Zahler AM, Williamson JR, Cech TR, Prescott DM. Inhibition of telomerase by G-quartet DNA structures. *Nature*. 1991;350(6320):718-20.
26. Zaug AJ, Podell ER, Cech TR. Human POT1 disrupts telomeric G-quadruplexes allowing telomerase extension in vitro. *Proc Natl Acad Sci U S A*. 2005;102(31):10864-9.
27. Gomez DL, Armando RG, Cerrudo CS, Ghiringhelli PD, Gomez DE. Telomerase as a Cancer Target. Development of New Molecules. *Curr Top Med Chem*. 2016;16(22):2432-40.
28. Sun D, Thompson B, Cathers BE, Salazar M, Kerwin SM, Trent JO, . . . Hurley LH. Inhibition of human telomerase by a G-quadruplex-interactive compound. *J Med Chem*. 1997;40(14):2113-6.
29. De Cian A, Cristofari G, Reichenbach P, De Lemos E, Monchaud D, Teulade-Fichou MP, . . . Mergny JL. Reevaluation of telomerase inhibition by quadruplex ligands and their mechanisms of action. *Proc Natl Acad Sci U S A*. 2007;104(44):17347-52.
30. Tippana R, Hwang H, Opresko PL, Bohr VA, Myong S. Single-molecule imaging reveals a common mechanism shared by G-quadruplex-resolving helicases. *Proc Natl Acad Sci U S A*. 2016;113(30):8448-53.
31. Budhathoki JB, Maleki P, Roy WA, Janscak P, Yodh JG, Balci H. A Comparative Study of G-Quadruplex Unfolding and DNA Reeling Activities of Human RECQ5 Helicase. *Biophys J*. 2016;110(12):2585-96.
32. Liu JQ, Chen CY, Xue Y, Hao YH, Tan Z. G-quadruplex hinders translocation of BLM helicase on DNA: a real-time fluorescence spectroscopic unwinding study and comparison with duplex substrates. *Journal of the American Chemical Society*. 2010;132(30):10521-7.
33. London TB, Barber LJ, Mosedale G, Kelly GP, Balasubramanian S, Hickson ID, . . . Hiom K. FANCD1 is a structure-specific DNA helicase associated with the maintenance of genomic G/C tracts. *J Biol Chem*. 2008;283(52):36132-9.
34. Moye AL, Porter KC, Cohen SB, Phan T, Zyner KG, Sasaki N, . . . Bryan TM. Telomeric G-quadruplexes are a substrate and site of localization for human telomerase. *Nat Commun*. 2015;6:7643.
35. Oganessian L, Moon IK, Bryan TM, Jarstfer MB. Extension of G-quadruplex DNA by ciliate telomerase. *Embo j*. 2006;25(5):1148-59.
36. Oganessian L, Graham ME, Robinson PJ, Bryan TM. Telomerase recognizes G-quadruplex and linear DNA as distinct substrates. *Biochemistry*. 2007;46(40):11279-90.
37. Lee HT, Bose A, Lee CY, Opresko PL, Myong S. Molecular mechanisms by which oxidative DNA damage promotes telomerase activity. *Nucleic Acids Res*. 2017;45(20):11752-65.

38. Palacky J, Vorlickova M, Kejnovska I, Mojzes P. Polymorphism of human telomeric quadruplex structure controlled by DNA concentration: a Raman study. *Nucleic Acids Res.* 2013;41(2):1005-16.
39. Petraccone L, Malafrente A, Amato J, Giancola C. G-quadruplexes from human telomeric DNA: how many conformations in PEG containing solutions? *J Phys Chem B.* 2012;116(7):2294-305.
40. Long X, Stone MD. Kinetic partitioning modulates human telomere DNA G-quadruplex structural polymorphism. *PLoS One.* 2013;8(12):e83420.
41. Dai J, Carver M, Punchihewa C, Jones RA, Yang D. Structure of the Hybrid-2 type intramolecular human telomeric G-quadruplex in K⁺ solution: insights into structure polymorphism of the human telomeric sequence. *Nucleic Acids Res.* 2007;35(15):4927-40.
42. Peng CG, Damha MJ. G-quadruplex induced stabilization by 2'-deoxy-2'-fluoro-D-arabinonucleic acids (2'F-ANA). *Nucleic Acids Res.* 2007;35(15):4977-88.
43. Lim KW, Amrane S, Bouaziz S, Xu W, Mu Y, Patel DJ, . . . Phan AT. Structure of the human telomere in K⁺ solution: a stable basket-type G-quadruplex with only two G-tetrad layers. *Journal of the American Chemical Society.* 2009;131(12):4301-9.
44. Abou Assi H, El-Khoury R, Gonzalez C, Damha MJ. 2'-Fluoroarabinonucleic acid modification traps G-quadruplex and i-motif structures in human telomeric DNA. *Nucleic Acids Res.* 2017;45(20):11535-46.
45. Byrd AK, Raney KD. A parallel quadruplex DNA is bound tightly but unfolded slowly by pif1 helicase. *J Biol Chem.* 2015;290(10):6482-94.
46. Gavathiotis E, Searle MS. Structure of the parallel-stranded DNA quadruplex d(TTAGGGT)₄ containing the human telomeric repeat: evidence for A-tetrad formation from NMR and molecular dynamics simulations. *Org Biomol Chem.* 2003;1:1650-6.
47. Lingner J, Hughes TR, Shevchenko A, Mann M, Lundblad V, Cech TR. Reverse transcriptase motifs in the catalytic subunit of telomerase. *Science.* 1997;276(5312):561-7.
48. Harrington L, Zhou W, McPhail T, Oulton R, Yeung DS, Mar V, . . . Robinson MO. Human telomerase contains evolutionarily conserved catalytic and structural subunits. *Genes Dev.* 1997;11(23):3109-15.
49. Weinrich SL, Pruzan R, Ma L, Ouellette M, Tesmer VM, Holt SE, . . . Morin GB. Reconstitution of human telomerase with the template RNA component hTR and the catalytic protein subunit hTERT. *Nat Genet.* 1997;17(4):498-502.
50. Counter CM, Meyerson M, Eaton EN, Weinberg RA. The catalytic subunit of yeast telomerase. *Proc Natl Acad Sci U S A.* 1997;94(17):9202-7.
51. Wyatt HD, Lobb DA, Beattie TL. Characterization of physical and functional anchor site interactions in human telomerase. *Mol Cell Biol.* 2007;27(8):3226-40.
52. Arthanari H, Basu S, Kawano TL, Bolton PH. Fluorescent dyes specific for quadruplex DNA. *Nucleic Acids Res.* 1998;26(16):3724-8.
53. Nicoludis JM, Barrett SP, Mergny JL, Yatsunyk LA. Interaction of human telomeric DNA with N-methyl mesoporphyrin IX. *Nucleic Acids Res.* 2012;40(12):5432-47.
54. Samosorn S, Tanwirat B, Muhamad N, Casadei G, Tomkiewicz D, Lewis K, . . . Bremner JB. Antibacterial activity of berberine-NorA pump inhibitor hybrids with a methylene ether linking group. *Bioorg Med Chem.* 2009;17(11):3866-72.

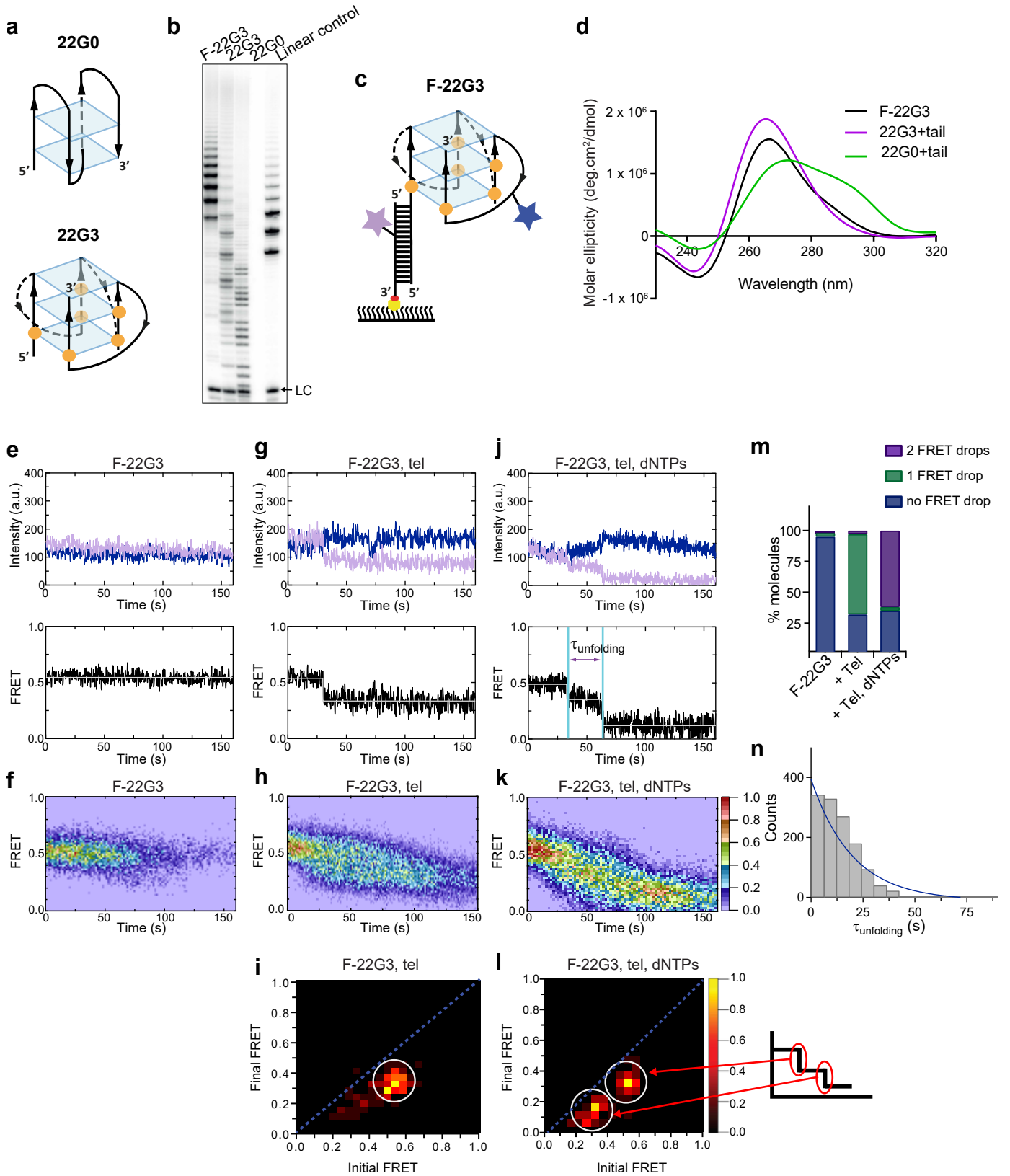
55. Samosorn S, inventor13-Arylalkyleneoxyberberine Derivatives as Anti-Breast Cancer Agents. Thailand2016.
56. De Cian A, Delemos E, Mergny JL, Teulade-Fichou MP, Monchaud D. Highly efficient G-quadruplex recognition by bisquinolinium compounds. *Journal of the American Chemical Society*. 2007;129(7):1856-7.
57. Chung WJ, Heddi B, Hamon F, Teulade-Fichou MP, Phan AT. Solution structure of a G-quadruplex bound to the bisquinolinium compound Phen-DC(3). *Angew Chem Int Ed Engl*. 2014;53(4):999-1002.
58. Ghosh S, Pradhan SK, Kar A, Chowdhury S, Dasgupta D. Molecular basis of recognition of quadruplexes human telomere and c-myc promoter by the putative anticancer agent sanguinarine. *Biochim Biophys Acta*. 2013;1830(8):4189-201.
59. Gray DM, Wen JD, Gray CW, Repges R, Repges C, Raabe G, Fleischhauer J. Measured and calculated CD spectra of G-quartets stacked with the same or opposite polarities. *Chirality*. 2008;20(3-4):431-40.
60. Hwang H, Kreig A, Calvert J, Lormand J, Kwon Y, Daley JM, . . . Myong S. Telomeric overhang length determines structural dynamics and accessibility to telomerase and ALT-associated proteins. *Structure*. 2014;22(6):842-53.
61. Wang F, Tang ML, Zeng ZX, Wu RY, Xue Y, Hao YH, . . . Tan Z. Telomere- and telomerase-interacting protein that unfolds telomere G-quadruplex and promotes telomere extension in mammalian cells. *Proc Natl Acad Sci U S A*. 2012;109(50):20413-8.
62. Paeschke K, Juraneck S, Simonsson T, Hempel A, Rhodes D, Lipps HJ. Telomerase recruitment by the telomere end binding protein-beta facilitates G-quadruplex DNA unfolding in ciliates. *Nat Struct Mol Biol*. 2008;15(6):598-604.
63. Postberg J, Tsytlonok M, Sparvoli D, Rhodes D, Lipps HJ. A telomerase-associated RecQ protein-like helicase resolves telomeric G-quadruplex structures during replication. *Gene*. 2012;497(2):147-54.
64. Birrento ML, Bryan TM, Samosorn S, Beck JL. ESI-MS Investigation of an Equilibrium between a Bimolecular Quadruplex DNA and a Duplex DNA/RNA Hybrid. *J Am Soc Mass Spectrom*. 2015;26(7):1165-73.
65. Chen MC, Tippiana R, Demeshkina NA, Murat P, Balasubramanian S, Myong S, Ferre-D'Amare AR. Structural basis of G-quadruplex unfolding by the DEAH/RHA helicase DHX36. *Nature*. 2018;558(7710):465-9.
66. Ray S, Qureshi MH, Malcolm DW, Budhathoki JB, Celik U, Balci H. RPA-mediated unfolding of systematically varying G-quadruplex structures. *Biophys J*. 2013;104(10):2235-45.
67. Qi X, Xie M, Brown AF, Bley CJ, Podlevsky JD, Chen JJ. RNA/DNA hybrid binding affinity determines telomerase template-translocation efficiency. *Embo j*. 2012;31(1):150-61.
68. Lacroix L, Seosse A, Mergny JL. Fluorescence-based duplex-quadruplex competition test to screen for telomerase RNA quadruplex ligands. *Nucleic Acids Res*. 2011;39(4):e21.
69. Nicoludis JM, Miller ST, Jeffrey PD, Barrett SP, Rablen PR, Lawton TJ, Yatsunyk LA. Optimized end-stacking provides specificity of N-methyl mesoporphyrin IX for human telomeric G-quadruplex DNA. *Journal of the American Chemical Society*. 2012;134(50):20446-56.
70. Gueddouda NM, Mendoza O, Gomez D, Bourdoncle A, Mergny JL. G-quadruplexes unfolding by RHAU helicase. *Biochim Biophys Acta Gen Subj*. 2017;1861(5 Pt B):1382-8.

71. Schaffitzel C, Berger I, Postberg J, Hanes J, Lipps HJ, Pluckthun A. In vitro generated antibodies specific for telomeric guanine-quadruplex DNA react with *Stylonychia lemnae* macronuclei. *Proc Natl Acad Sci U S A*. 2001;98(15):8572-7.
72. Paeschke K, Simonsson T, Postberg J, Rhodes D, Lipps HJ. Telomere end-binding proteins control the formation of G-quadruplex DNA structures in vivo. *Nat Struct Mol Biol*. 2005;12(10):847-54.
73. Zhang ML, Tong XJ, Fu XH, Zhou BO, Wang J, Liao XH, . . . Zhou JQ. Yeast telomerase subunit Est1p has guanine quadruplex-promoting activity that is required for telomere elongation. *Nat Struct Mol Biol*. 2010;17(2):202-9.
74. Murat P, Balasubramanian S. Existence and consequences of G-quadruplex structures in DNA. *Curr Opin Genet Dev*. 2014;25:22-9.
75. Bao HL, Liu HS, Xu Y. Hybrid-type and two-tetrad antiparallel telomere DNA G-quadruplex structures in living human cells. *Nucleic Acids Res*. 2019;47(10):4940-7.
76. Liu HY, Zhao Q, Zhang TP, Wu Y, Xiong YX, Wang SK, . . . Huang ZS. Conformation Selective Antibody Enables Genome Profiling and Leads to Discovery of Parallel G-Quadruplex in Human Telomeres. *Cell chemical biology*. 2016;23(10):1261-70.
77. Sen D, Gilbert W. Formation of parallel four-stranded complexes by guanine-rich motifs in DNA and its implications for meiosis. *Nature*. 1988;334(6180):364-6.
78. Tomlinson CG, Sasaki N, Jurczyk J, Bryan TM, Cohen SB. Quantitative assays for measuring human telomerase activity and DNA binding properties. *Methods*. 2017;114:85-95.
79. Cohen SB, Reddel RR. A sensitive direct human telomerase activity assay. *Nat Methods*. 2008;5(4):355-60.

1 **Figure legends**

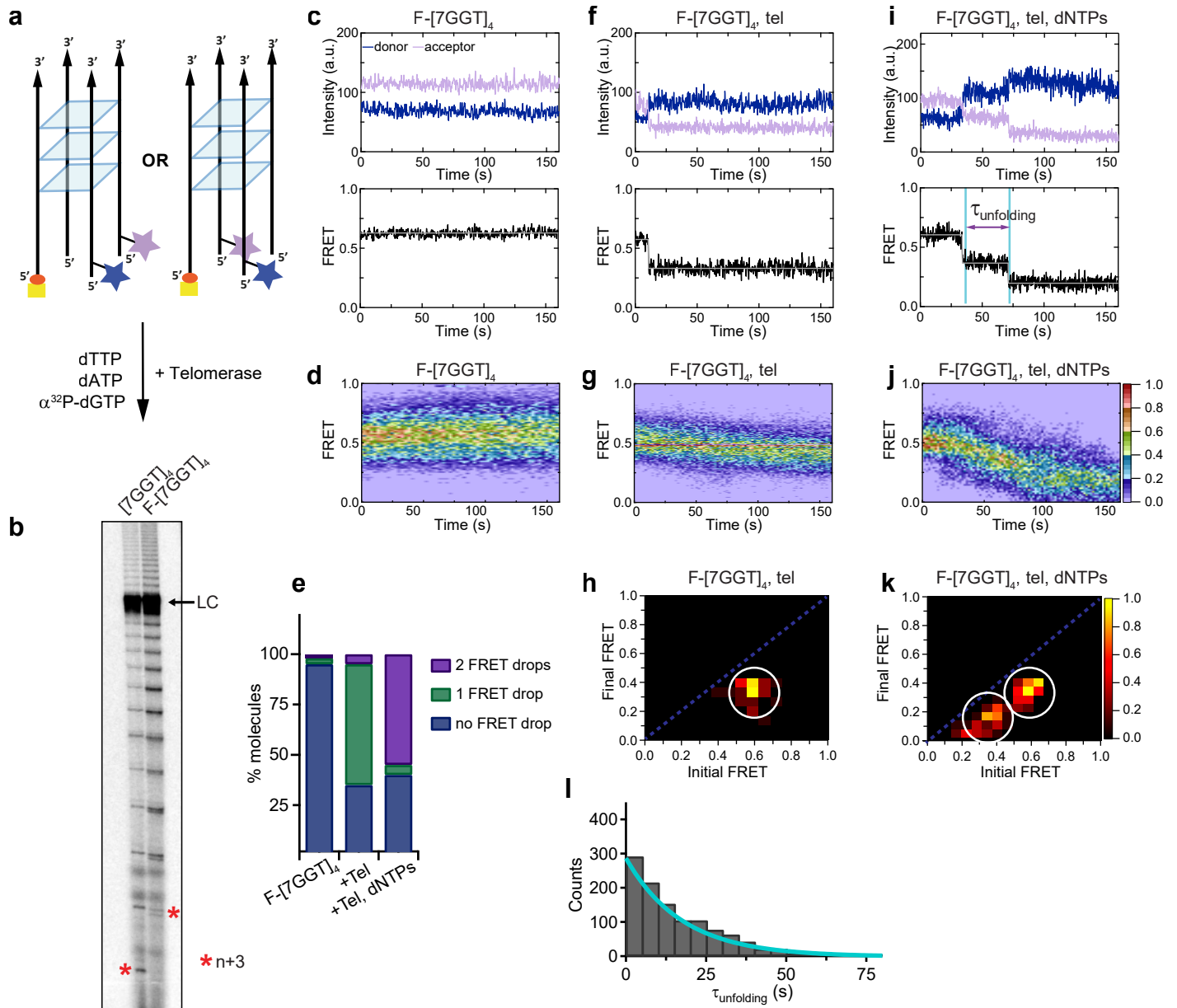
2 **Figure 1: Telomerase unfolds and extends a parallel G-quadruplex.** (a) Schematic of the
3 likely topology of (top) an antiparallel G-quadruplex formed from unmodified telomeric 22-
4 mer 22G0 and (bottom) a parallel unimolecular G-quadruplex formed from a telomeric 22-
5 mer with 2'F-araG in the indicated positions (orange circles). (b) Telomerase extension assays
6 in the presence of radiolabeled dGTP ($\alpha^{32}\text{P}$ -dGTP). The extension products of 2 μM each of
7 fluorescently-labeled 22G3 (F-22G3), unlabeled 22G3, unmodified 22G0 and linear control
8 oligonucleotide Bio-L-18GGG (see Supplementary Table 1) were analyzed using denaturing
9 polyacrylamide gel electrophoresis. LC: 5'- ^{32}P -labeled synthetic 12 nt DNA used as a
10 recovery/loading control. (c) The F-22G3 FRET construct, showing the positions of the FRET
11 dye pair and biotin for immobilization onto the functionalized coverslip. Blue star: AlexaFluor
12 555TM (donor dye); purple star: AlexaFluor 647TM (acceptor dye); orange circles: 2'F-araG; red
13 circle: biotin; yellow circle: Neutravidin. (d) CD spectra of G4 (20 μM) formed from 2'F-araG-
14 modified 5'-extended 22G3 labeled with a FRET dye (22G3+tail), and the same G4 after
15 hybridization to a second oligonucleotide bearing a second FRET dye (F-22G3). A peak at 265
16 nm is characteristic of parallel G4; the slight shoulder at ~290 nm in the F-22G3 spectrum is
17 attributable to duplex DNA since it is absent from the spectrum of 22G3+tail. 22G0+tail is a
18 control oligonucleotide of equal length and base composition to 22G3+tail, but with no 2'F-
19 ara G substitutions or conjugated dye. (e),(g),(j) Representative single-molecule acceptor
20 (purple) and donor (blue) intensities of F-22G3 molecules over time (top panels), and the FRET
21 traces (bottom panels) representing the ratio of acceptor intensity to the sum of acceptor and
22 donor intensities, of either F-22G3 alone (e), in the presence of telomerase (g), or in the
23 presence of telomerase and dNTPs (j). (f),(h),(k) Heat maps of the distribution of FRET
24 intensities over 0 - 150 s of F-22G3, either alone (n = 99) (f), in the presence of telomerase (n
25 = 125) (h), or in the presence of telomerase and dNTPs (n = 90) (k). All plots include molecules
26 collected in 4 – 6 independent experiments. For color key, see panel (k). (i),(l) TDPs showing
27 the change in FRET value of molecules from experiments in (h) and (k) (n = 90 and 75,
28 respectively). Schematic in (l) shows assignment of each TDP peak to one of the two steps of
29 FRET reduction observed in single molecule traces. (m) Plot of the percentage of molecules
30 showing no change in FRET, a single FRET drop, or a two-step FRET drop, in the experiments
31 shown in (e-l). (n) The unfolding rate of F-22G3, calculated by fitting the dwell time
32 distributions of the intermediate FRET state (see panel j) to a single exponential equation (n =
33 76 molecules).

Figure 1



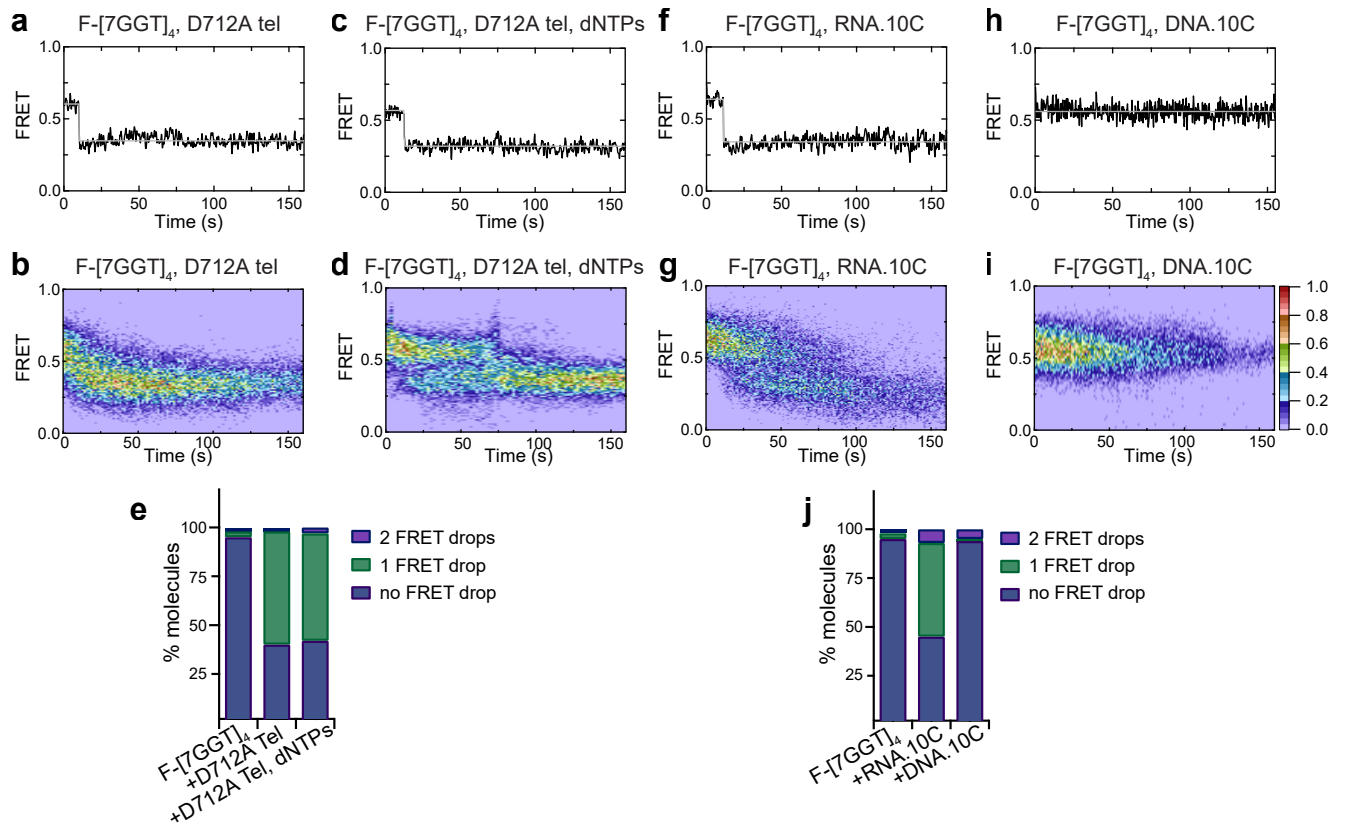
1 **Figure 2: Telomerase unfolds and extends a tetrameric parallel G-quadruplex. (a)**
2 Schematic representation of F-[7GGT]₄ used in smFRET studies. Blue star: AlexaFluor 555TM
3 (donor dye); purple star: AlexaFluor 647TM (acceptor dye); red circle: biotin; yellow square:
4 Neutravidin. **(b)** Telomerase extension assays using either 1 μM of unmodified [7GGT]₄ or the
5 version containing the FRET pair dyes (F-[7GGT]₄); radiolabeled extension products were
6 electrophoresed on a denaturing polyacrylamide gel (* indicates the position of n+3 products
7 in the gel). LC: 5'-³²P-labeled synthetic 100 nt DNA used as a recovery/loading control.
8 **(c),(f),(i)** Representative single-molecule acceptor (purple) and donor (blue) intensities of F-
9 [7GGT]₄ molecules over time (top panels), and the corresponding FRET traces (bottom
10 panels). **(d),(g),(j)** Heat maps of the distribution of FRET intensities over 0 - 150 s. For color
11 key, see panel **(j)**. Panels **(c)** and **(d)** represent F-[7GGT]₄ alone (n = 105 molecules), **(f)** and
12 **(g)** show F-[7GGT]₄ in the presence of telomerase (n = 87), and **(i)** and **(j)** show F-[7GGT]₄ in
13 the presence of telomerase and dNTPs (n = 81). All plots include molecules collected in 4 – 6
14 independent experiments. **(e)** Plot of the percentage of molecules showing no change in FRET,
15 a single FRET drop, or a two-step FRET drop, in the experiments shown above. **(h),(k)**
16 Transition density plots (TDPs) depicting initial and final FRET states of all molecules that
17 showed a change in FRET value, in the presence of telomerase (n = 65) **(h)** or telomerase and
18 dNTPs (n = 75) **(k)**. For color key, see panel **(k)**. **(l)** Plot of the dwell time distribution at the
19 0.36 FRET state for 55 molecules from experiment in **(i-k)**, representing the rate of telomerase-
20 mediated G4 unfolding.

Figure 2



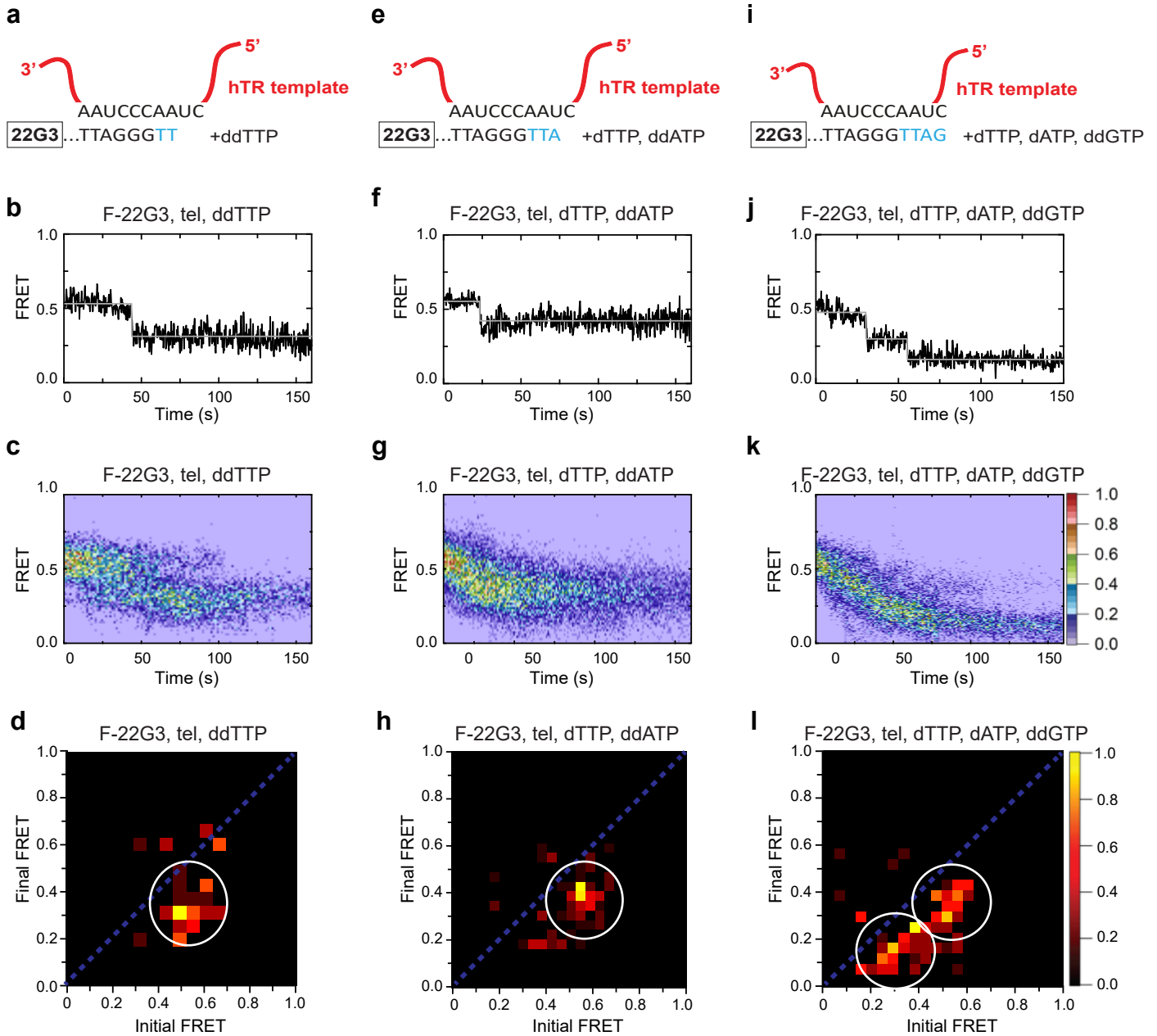
1 **Figure 3: Partial unfolding of G4 does not require telomerase catalytic activity, and can**
2 **be induced by the RNA template. (a),(c),(f),(h)** Examples of individual F-[7GGT]₄ FRET
3 traces under the indicated experimental conditions over 160 s. **(b),(d),(g),(i)** Heat maps of the
4 distribution of FRET trajectories over 0 - 150 s using 80, 75, 95 and 129 molecules,
5 respectively, under the indicated experimental conditions. All plots include molecules collected
6 in 4 – 6 independent experiments. For color key, see panel **(i)**. **(e),(j)** Plots of the percentage
7 of molecules showing no change in FRET, a single FRET drop, or a two-step FRET drop, in
8 the experiments shown above.

Figure 3



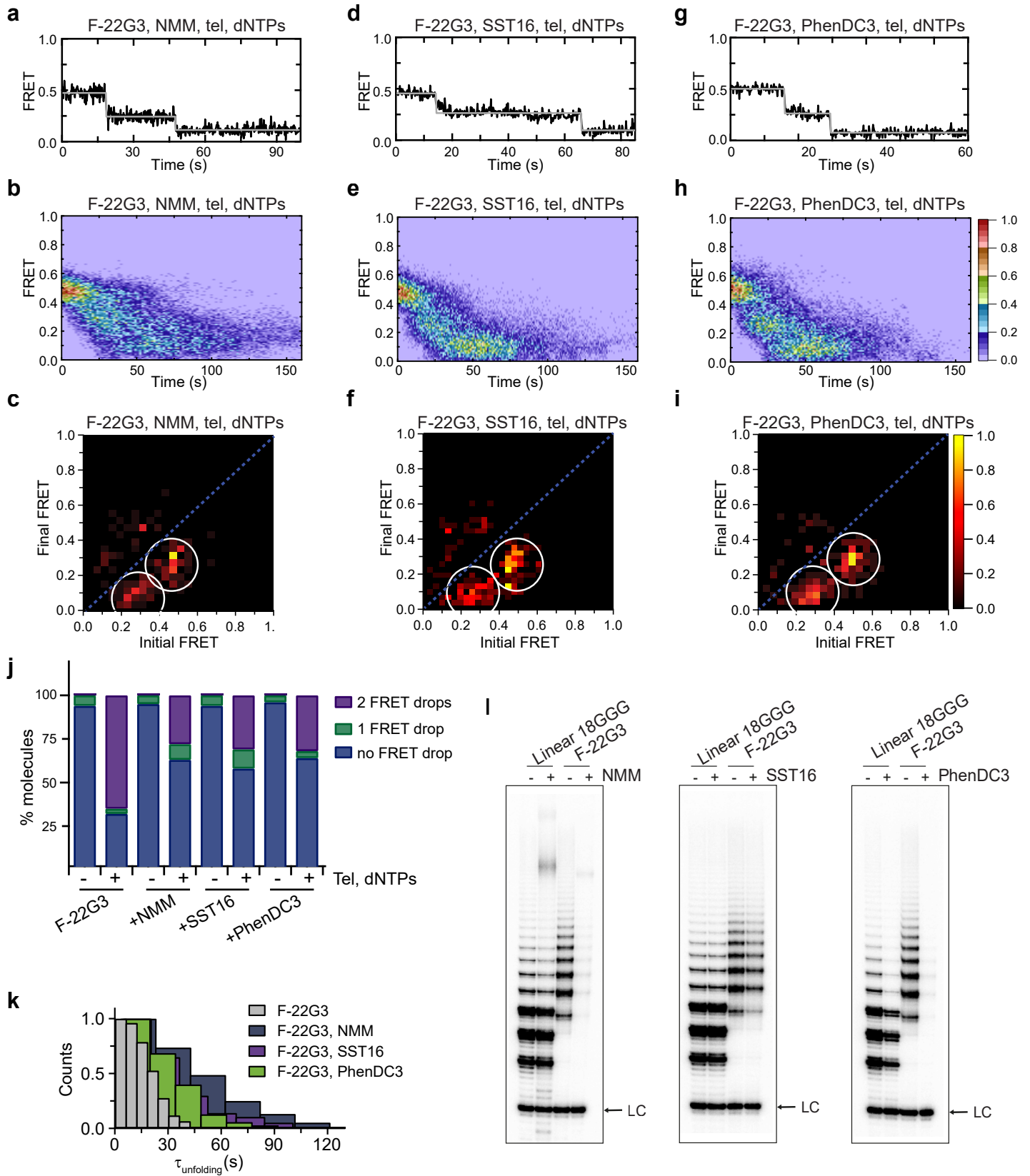
1 **Figure 4: Telomerase translocation leads to complete G4 unfolding.** (a),(e),(i) Schematic
2 diagrams showing alignment of the telomerase template RNA with 22G3 DNA and template-
3 directed incorporation of ddTTP (a), dTTP followed by ddATP (e) or dTTP, dATP and ddGTP
4 (i). (b),(f),(j) Examples of individual F-22G3 FRET trajectories in the presence of telomerase
5 and the indicated combinations of nucleotides. (c),(g),(k) Heat maps of the distribution of
6 FRET intensities over 0 - 150 s in 80, 90 and 82 molecules, respectively, in the presence of
7 telomerase and the indicated combinations of nucleotides. All plots include molecules collected
8 in 4 – 6 independent experiments. For color key, see panel (k). (d),(h),(l) TDPs showing the
9 changes between the initial and final FRET values of F-22G3 in the presence of telomerase and
10 the indicated combinations of nucleotides (n = 80, 90 and 82 molecules, respectively). For color
11 key, see panel (l).

Figure 4



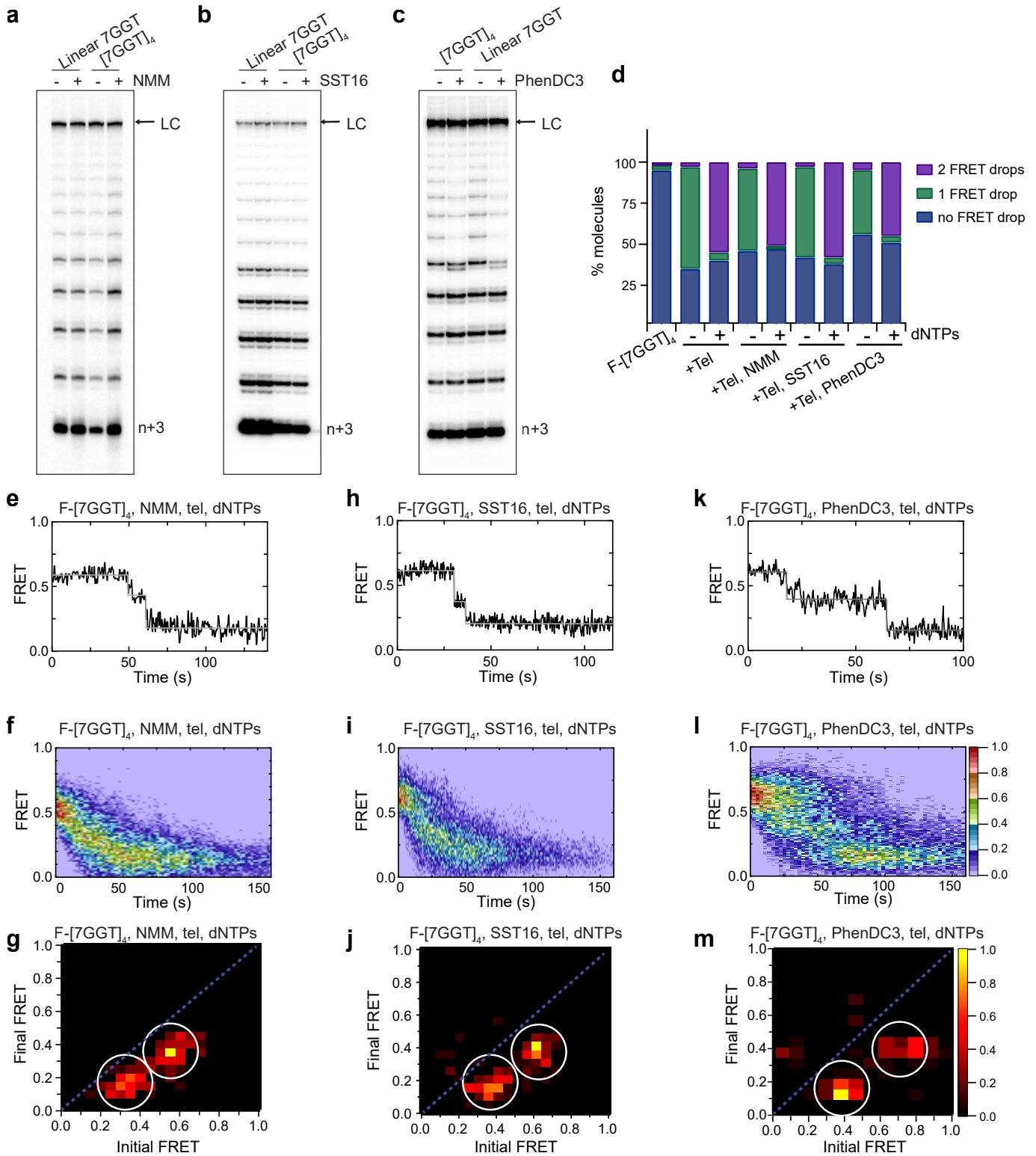
1 **Figure 5: Partial inhibition of unfolding of F-22G3 by ligands NMM, SST16 and**
2 **PhenDC3. (a – i)** Representative FRET trajectories, heat maps and transition density plots of
3 F-22G3 in the presence of NMM (**a – c**; 800 μ M in folding reaction), SST16 (**d – f**; 5 μ M) or
4 PhenDC3 (**g – i**; 1 μ M), in the presence of telomerase and dNTPs; n = 84 (**b,c**), 60 (**e,f**), and
5 77 (**h,i**) molecules, collected in 2-4 independent experiments. (**j**) Plot of the percentage of F-
6 22G3 molecules showing no change in FRET, a single FRET drop, or a two-step FRET drop,
7 when incubated with telomerase, dNTPs and the indicated ligands at the concentrations shown
8 in (**a – i**). (**k**) The unfolding rate of F-22G3 in the presence of the above concentrations of
9 NMM, SST16, PhenDC3 or no ligand, calculated by fitting the dwell time distributions of the
10 intermediate FRET state to a single exponential equation. n = 76 (no ligand), 84 (NMM), 60
11 (SST16) and 77 (PhenDC3). (**l**) Telomerase extension assays using 250 nM of F-22G3 or linear
12 Bio-L-18GGG control, in the presence or absence of NMM, SST16 or PhenDC3 at the
13 concentrations above. For the reactions with NMM, linear DNA strands (10 μ M) were
14 incubated with 800 μ M NMM prior to G4 folding, and the G4-ligand complex diluted 20-fold
15 for the activity assay. LC: 5'-³²P-labeled synthetic 30 nt DNA used as a recovery/loading
16 control.

Figure 5



1 **Figure 6: Telomerase unfolds and extends ligand-stabilized tetrameric parallel G4.**
2 **(a),(b),(c)** Telomerase extension assays using 1 μM of $[\text{7GGT}]_4$ or a linear 7-mer control (or
3 250 nM in the reactions with PhenDC3), in the presence or absence of 40 μM NMM **(a)**, 100
4 μM SST16 **(b)** or 1 μM PhenDC3 **(c)**. For the reactions with NMM, linear 7GGT (1 mM) was
5 incubated with 10 mM NMM prior to G4 folding, and the G4-ligand complex diluted 250-fold
6 for the activity assay. n+3 indicates the position of the product with the first 3 nucleotides
7 incorporated. LC: 5'- ^{32}P -labeled synthetic 100 nt DNA used as a recovery/loading control. **(d)**
8 Plot of the percentage of F- $[\text{7GGT}]_4$ molecules showing no change in FRET, a single FRET
9 drop, or a two-step FRET drop, when incubated with telomerase and the indicated ligands at
10 the concentrations shown in **(a) – (c)**. **(e),(h),(k)** Representative single-molecule FRET
11 trajectories of NMM-stabilized **(e)**, SST16-stabilized **(h)** or PhenDC3-stabilized **(k)** F-
12 $[\text{7GGT}]_4$ in the presence of telomerase and dNTPs. **(f),(i),(l)** Heat maps of the distribution of
13 FRET intensities over 0 - 150 s in the presence of telomerase, dNTPs and either NMM (n = 63)
14 **(f)**, SST16 (n = 90) **(i)** or PhenDC3 (n = 76) **(l)**. All plots include molecules collected in 4 – 6
15 independent experiments. For color key, see panel **(l)**. **(g),(j),(m)** TDPs showing the changes
16 in FRET value of 70, 80 and 58 molecules from the experiments in **(e)** to **(l)**.

Figure 6



- 1 **Figure 7:** A proposed model for parallel G4 extension and unfolding by human telomerase.
- 2 See text for details.

Figure 7

